PREPARATION AND CHARACTERIZATION OF MAGNETIC NANOPARTICLES

A THESIS SUBMITTED TO
THE GRADUATE SCHOOL OF NATURAL AND APPLIED SCIENCES
OF
MIDDLE EAST TECHNICAL UNIVERSITY

BY

BURCU KÜÇÜK

IN PARTIAL FULFILLMENT OF THE REQUIREMENTS
FOR
THE DEGREE OF MASTER OF SCIENCE
IN
CHEMISTRY

JUNE 2009

Approval of the thesis:

PREPARATION AND CHARACTERIZATION OF MAGNETIC NANO PARTICLES

submitted by **BURCU KÜÇÜK** in partial fulfillment of the requirements for the degree of **Master of Science in Chemistry Department, Middle East Technical University** by,

Prof. Dr. Canan Özgen
Dean, Graduate School of **Natural and Applied Sciences** _____

Prof. Dr. Ahmet M. Önal
Head of Department, **Chemistry** _____

Prof. Dr. Mürvet Volkan
Supervisor, **Chemistry Department, METU** _____

Prof. Dr. Macit Özenbaş
Co-supervisor, **Metalurgical and Mater. Eng. Dept., METU** _____

Examining Committee Members:

Prof. Dr. O. Yavuz Ataman
Chemistry Dept., METU _____

Prof. Dr. Macit Özenbaş
Metalurgical and Materials Engineering Dept., METU _____

Prof. Dr. E. Hale Göktürk
Chemistry Dept., METU _____

Prof. Dr. Mürvet Volkan
Chemistry Dept., METU _____

Assoc. Prof. Nursen Çoruh
Chemistry Dept., METU _____

Date: June 30, 2009

I hereby declare that all information in this document has been obtained and presented in accordance with academic rules and ethical conduct. I also declare that, as required by these rules and conduct, I have fully cited and referenced all material and results that are not original to this work.

Name, Last Name: BURCU KÜÇÜK

Signature :

ABSTRACT

PREPARATION AND CHARACTERIZATION OF MAGNETIC NANOPARTICLES

Küçük, Burcu

M.S., Department of Chemistry
Supervisor: Prof. Dr. Mürvet Volkan
Co-supervisor: Prof. Dr. Macit Özenbaş

June 2009, 84 pages

Magnetite (Fe_3O_4) and Maghemite (γ-Fe_2O_3) are well-known iron oxide phases among magnetic nanoparticles due to their magnetic properties, chemical stability, and nontoxicity. They have gained acceptance in several fields of application of nanomaterials such as magnetic recording systems, magnetic refrigeration, magneto-optical devices, magnetic resonance imaging, magnetic separation techniques and separation and purification of biological molecules.

Recently, there is a growing interest in the synthesis of magnetic iron oxide nanoparticles in a polymeric, glassy or ceramic matrix since the preparation of pure phase iron oxide composite material involves, presently, some difficulties partially arising from different oxidation states of iron which can lead to the presence of various oxides. Matrix support, in principle, modifies the properties of nanomaterials, thus opening new possibilities for the control of their performance. In

addition, the chosen matrix, polymer or sol-gel, provides binding of the functional groups and also prevents grain growth and agglomeration. Therefore, extensive research is conducted on this subject.

Sonochemical technique is an effective method to synthesize magnetic nanoparticles with many unique properties due to extreme reaction conditions. Besides, a microscopic mixing in the synthesis procedure is obtained because of the microjet effect which comes from the collapse of the bubbles. This effect creates relatively uniform reaction conditions. Thus, well-dispersed and stable nanoparticles are obtained by using ultrasound.

In this study, γ-Fe_2O_3, maghemite nanoparticles are accommodated in an inert, inorganic, transparent and temperature resistant sol gel matrix to achieve stabilization. The nature and concentration of the salt used, evaporation conditions of the sols, the following heat treatments had been investigated and shown that they had great influence on the particle size and the final iron oxide phase in the sol-gel. The Fe_2O_3/SiO_2 nanocomposites were characterized using X-ray diffraction (XRD) and vibrating sample magnetometry (VSM) techniques.

In addition, magnetite (Fe_3O_4) nanoparticles were synthesized via co-precipitation in the presence of poly(methacrylic acid) (PMAA) in aqueous solution. PMAA, which was used as the coating material, prevents magnetite nanoparticles from oxidation towards a lower saturation magnetization iron oxide phases. In order to achieve small particle size and uniform size distribution of the magnetite nanoparticles in PMAA matrix, ultrasonic irradiation was applied during co-precipitation. The polymer coated Fe_3O_4 nanoparticles were characterized using scanning electron microscopy (SEM), laser particle sizer, X-ray diffraction, (XRD) and vibrating sample magnetometry (VSM) techniques and zeta potential measurements.

Keywords: magnetite, maghemite, iron oxide, magnetic, nanoparticles, poly(methacrylic) acid, sol-gel, polymer coating, ultrasonic

ÖZ

MANYETİK NANOTANECİKLERİNİN HAZIRLANMASI VE KARAKTERİZASYONU

Küçük, Burcu

Yüksek Lisans, Kimya Bölümü
Tez Yöneticisi: Prof. Dr. Mürvet Volkan
Ortak Tez Yöneticisi: Prof. Dr. Macit Özenbaş

Haziran 2009, 84 sayfa

Manyetik özellikleri, kimyasal kararlılıkları ve toksik olmamaları nedeni ile Magnetit (Fe_3O_4) ve Maghemit (γ-Fe_2O_3) manyetik nanotanecikler arasında iyi bilinen demir oksit fazlarıdır. Nanomalzemelerin kullanıldığı manyetik kaydetme sistemleri, manyetik soğutma, manyeto-optik aygıtlar, manyetik rezonans görüntüleme, manyetik ayırma teknikleri ve biyolojik moleküllerin ayırımı ve saflaştırılması gibi pek çok uygulama alanında kabul görmüşlerdir.

Son zamanlarda, saf faz nano demir oksit kompozit maddesinin elde edilmesinde farklı oksitlenme basamaklarının birden fazla oksit oluşumuna neden olmasıyla ilgili zorluklar sebebiyle, manyetik demir oksit nanotaneciklerinin cam, seramik veya polimer matriksler içinde sentezlenmesi giderek artan bir ilgi görmektedir. Hazırlanan kristalin özellikleri içinde bulunduğu ortama bağlı olarak değişebildiği için matris seçimi kristalin genel performansını kontrol etmek açısından yeni

olasılıklar barındırmaktadır. Ayrıca seçilen matris, polimer ya da sol-jel, fonksiyonel gruplara bağlanma sağlar ve tanecik büyümesini ve topaklanmayı önler. Bu nedenle, konu ile ilgili kapsamlı araştırmalar yapılmıştır.

Sonokimyasal teknik, aşırı reaksiyon şartlarından kaynanklanan bir çok eşsiz özelliği ile manyetik naotanecik sentezlemede etkili bir yöntemdir. Ayrıca gaz kabarcıklarının patlamasından gelen mikrojet etkisi sebebi ile sentez sürecinde mikroskobik bir karıştırma elde edilir. Bu etki, göreceli olarak homojen reaksiyon şartları oluşturur ve ultrasonik uyarma ile iyi dağılmış ve kararlı nanotanecikler elde edilebilir.

Bu çalışmada stabilizasyonu sağlamak için maghemit (γ-Fe_2O_3) nanotanecikleri inert, anorganik, saydam ve ısıya dayanıklı sol-jel matrisinin içinde sentezlendi. Kullanılan tuzun doğası ve konsantrasyonu, buharlaştırma şartları ve takip eden ısı uygulamaları incelenerek bunların sol-jel içindeki demir oksitin fazı ve parçacık boyutu üzerinde büyük etkisi olduğu gösterilmiştir. Fe_2O_3/SiO_2 nanokompozitlerin karakterizasyonu X-ışını kırımını (XRD) ve titreşen örnek magnetometresi (VSM) teknikleri kullanılarak yapılmıştır.

Ayrıca, magnetit (Fe_3O_4) nanotanecikleri sulu çözeltide polimetakrilik asit (PMAA) ile birlikte çökme tekniği ile sentezlenmiştir. Kaplama malzemesi olarak PMAA'in kullanılması magnetit nanotaneciklerinin daha düşük doygunluk mıknatıslanmasına (saturation magnetization) sahip demir oksit fazlarına doğru oksitlenmesini engellemektedir. PMAA matrisindeki magnetit nanotanecikleri için küçük tanecik boyutuna ve bir örnek boyut dağılımına ulaşmak amacıyla birlikte çökme sırasında ultrasonik uyarma uygulanmıştır. Polimer kaplı Fe_3O_4 nanotaneciklerinin karakterizasyonu taramalı elektron mikroskobu (SEM), laser parçacık boyutu analizi, X-ışını kırımını (XRD), titreşen örnek magnetometresi (VSM) teknikleri ve zeta potansiyel ölçümleri kullanılarak yapılmıştır.

Anahtar Kelimeler: magnetit, maghemit, demir oksit, manyetik, nanotanecik, polimetakrilik asit, sol-jel, polimer kaplama, ultrasonik

To my grandmother, *Melek*

ACKNOWLEDGEMENTS

Words fail me to express my feelings of gratitude to my supervisor Prof. Dr. Mürvet Volkan for her enthusiastic guidance, encouragement and patience throughout the study. It would be very troublesome for me to finish my thesis work if she did not welcome me back and not rely on me at every stage of this thesis.

I would like to thank to my co-supervisor, Prof. Dr. Macit Özenbaş for his valuable guidance and criticism throughout the study. I am also deeply grateful to Assoc. Prof. Dr. Necati Özkan for his support, guidance and valuable instructions during this study.

My special thanks go to the Team; Seda Kibar, Ceren Uzun, Ümit Zengin and Barış Tanrıkulu; for their continuous help during my study, their valuable discussions, their great computer skills and most importantly their honest friendships. I am aware that it had been a tiring period to cope with the centrifuge tubes and moreover to deal with me. I am very grateful also to Nehir Güler, one of the most important person who encouraged me to keep on during this study.

I would like to thank to all my lab mates in C-50 Analytical Chemistry Laboratory, first Murat Kaya, then Bahar Köksel, Gülfem Aygar, Mervegül Maden, Recep Yüksel, Seher Karabıçak, Sezen Keser, Tuğba Nur Alp, Üzeyir Doğan, Zehra Tatlıcı and Zeynep Ergül, for their kind supports and warm friendships which created a great atmosphere.

Finally, my special appreciation and gratitude are devoted to my mother, Mübeşşer Küçük, my father, Veysel Nedim Küçük and my little sister, Hilal Küçük for their trust, patience and moral support, which made everything possible. Without them, I would not have the courage and the chance to reach an end for this study.

TABLE OF CONTENTS

LIST OF TABLES

TABLES

LIST OF FIGURES

FIGURES

CHAPTER 1

INTRODUCTION

Nano (symbol n) is a prefix in the International System of Units denoting a factor of 10^{-9} or 0.000000001. The prefix is derived from Greek, meaning dwarf, and was officially confirmed as standard in 1960. When used as a prefix for something other than a unit of measure, as in "nanoscience", nano means relating to nanotechnology.

Nanotechnology, shortened to "Nanotech", is the study of the control of matter on an atomic and molecular scale. Generally nanotechnology deals with structures of the size 100 nanometers or smaller, and involves developing materials or devices within that size. Nanotechnology is very diverse, ranging from novel extensions of conventional device physics, to completely new approaches based upon molecular self-assembly, to developing new materials with dimensions on the nanoscale, even to speculation on whether matter can be directly controlled on the atomic scale.

1.1 Nanotechnology

1.1.1 The Overview for Nanotechnology

The first use of the concepts in 'nano-technology' was in 'There's Plenty of Room at the Bottom' [1], a talk given by Richard Feynman at an American Physical Society meeting at Caltech on December 29, 1959. Richard Feynman was an American physicist known for quantum mechanics, the theory of quantum electrodynamics and the physics of the superfluidity, as well as work in particle physics. For his contributions to the development of quantum electrodynamics, Feynman received the

Nobel Prize in Physics in 1965. In his mind-blowing talk, ‘There's Plenty of Room at the Bottom’, Feynman described a process by which the ability to manipulate individual atoms and molecules might be developed, using one set of precise tools to build and operate another proportionally smaller set, so on down to the needed scale while claiming why the entire 24 volumes of the Encyclopaedia Britannica can not be written on the head of a pin. In the course of this, he asked if the atoms could be arranged one by one the way we want them and noted scaling issues would arise from the changing magnitude of various physical phenomena: gravity would become less important, surface tension and Van der Waals attraction would become more important, etc.

The term ‘nanotechnology’ was first defined in 1974 by Tokyo Science University Professor Norio Taniguchi as follows: ‘'Nano-technology' mainly consists of the processing of, separation, consolidation, and deformation of materials by one atom or by one molecule.’ [2].

In 1981, K. Eric Drexler, a Massachusetts Institute of Technology trained engineer, wrote a paper in which he proposed building machines by a ‘bottom-up’ approach that used ‘molecular assemblers’ to manipulate individual atoms [3]. In 1986, the term ‘nanotechnology’ reached greater public awareness with the publication of ‘Engines of Creation: The Coming Era of Nanotechnology’, the first book on the topic of nanotechnology, by Eric Drexler.

There have been two major developments in the early of 1980s. The first was the birth of cluster science. In 1985, Harold Kroto, James R. Heath, Sean O'Brien, Robert Curl and Richard Smalley discovered buckyball cluster, C_{60}, and shortly thereafter came to discover the fullerenes. The second major development was invention of scanning tunneling microscopy (STM) in 1981 by Gerd Binnig and Heinrich Rohrer (at IBM Zurich), who earned the Nobel Prize in Physics later in 1986. With this technology, individual atoms could be clearly identified for the first time. STM was essential for the development of the field of nanotechnology because what had been previously concepts were now within view and testable. Gerd Binnig,

Quate and Gerber invented the first Atomic Force Microscope (AFM) in 1986. The AFM is one of the foremost tools for imaging, measuring and manipulating matter at the nanoscale.

By concerning the reality of nanotechnology, NASA started to study about computational molecular nanotechnology in 1996. The National Science and Technology Council (NSTC) of the United States of America created the Interagency Working Group on Nanoscience Engineering and Technology (IWGN) in 1998. In January 2000, The U.S. National Nanotechnology Initiative (NNI) was established.

The 2007 Nobel Prize in Physics, which was the first Nobel Prize awarded to a genuine form of nanotechnology, was awarded to Albert Fert (Université Paris-Sud, Orsay, France) and Peter Grünberg (Institut für Festkkörperforschung, Jülich, Germany) for discovering the 'Giant Magnetoresistance' (GMR).

Nowadays, nanotechnology is referred as 'one of the key technologies that triggered the Third Industrial Revolution' [4] and will impact the future development in many areas related to health and medicine, environment and energy, materials and manufacturing, nanoelectronics and computer technology, biotechnology and agriculture, science and education, aeronautics and space exploration, national security, and global trade and competitiveness [4].

International Risk Governance Council (IRGC) published a policy brief describing the four generations of nanotechnology development as shown in Table 1.1 [5, 6]. According to the IRGC, the first generation is that of passive nanostructures. The main applications are intermediary system components such as particles, wires, nanotubes and nanolayers. The second phase, which just entering, introduces active nanostructures for multitasking. Typical applications are expected to be in device and system components such as sensors with a reacting actuator or drug delivery multi-component particles that change their structure as they reach their intended target. The third generation is expected to begin emerging around 2010. The synthesis and assembly techniques will allow for: forms of multiscale chemical and bio-assembly;

networking at the nanoscale; and scaled and hierarchical structures. In nanomedicine, this could mean the development of artificial organs and scaffolds for skin tissues. A few years after that, during fourth generation, the system components and devices are reduced to molecules and supramolecular structures that have specific structures and play different roles within the nanosystem. Potential applications include nanoscale genetic therapies and supramolecular components for transistors.

Table 1.1 Four generations of products and production processes on nanotechnology proposed by IRGC [5]

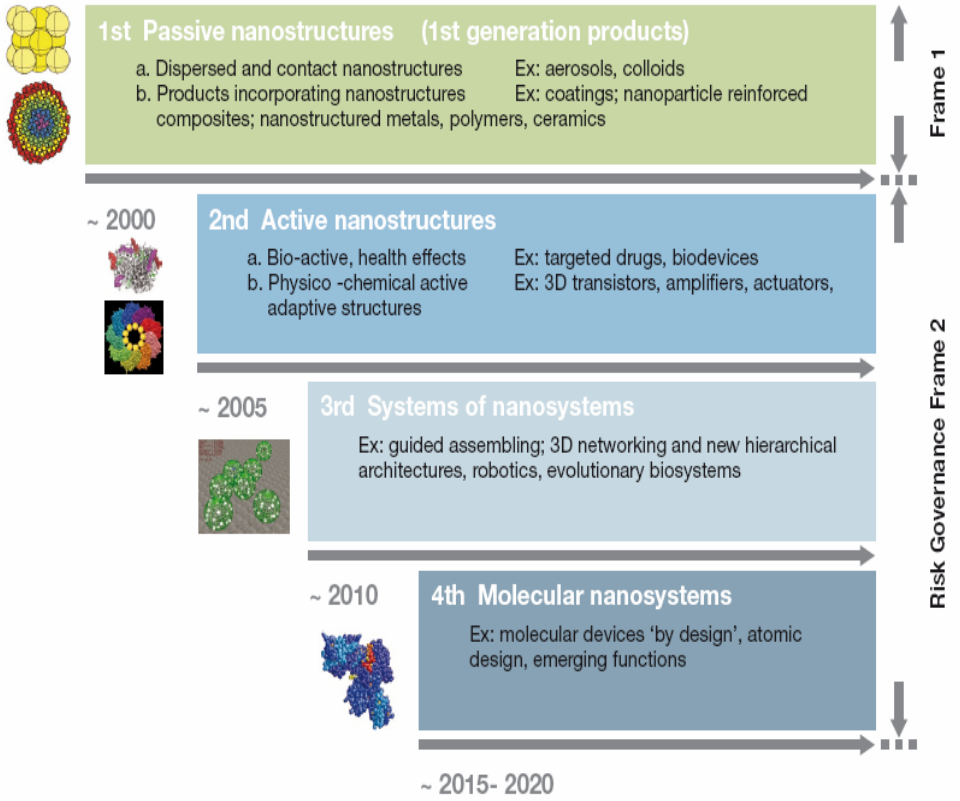

Nanotechnology refers to measurement or visualization at the scale of 1-100 nanometers. But the definition of Center for Responsible Nanotechnology (CRN) seems to be more precise than that. According to CRN, it will become increasingly obvious that engineering of functional systems at the molecular scale' [7] is what nanotechnology is really about as time passes through the four generations of nanotechnology.

1.1.2 The Applications of Nanotechnology

Nanotechnology offers a lot of benefits for various kinds of applications as it improves at diverse range of fields. The applications summarized under various topics can be observed at Table 1.2.

Table 1.2 Nanotechnology applications [8]

Catalysts	Photo, Electro, Platinum, Bimetallic, Oxide
Lasers	Deposition, Ablation, Sapphire, Excimer, Semiconductor, Laser Tweezers, Desorption Ionization, Quantum Dot, Vertical-Cavity Surface-Emitting, Pump, Distributed Feedback, Solid-State, Quantum Cascade, Quantum Well, Edge-Emitting, Waveguide, Matrix Assisted
Sensors	Glucose/Amperometric/SPR/DNA Biosensors, Immunosensors, Gas, Chemical, Optical, Pressure, Electrochemical, Temperature, pH, Humidity, Oxygen, Force
Electrodes	Gold, Glassy Carbon, Gate, Composite, Graphite, Platinum, ITO, TiO_2, Enzyme, Ferromagnetic, Carbon Paste, Diamond, Calomel, Photo, CNT, SnO_2, BDD, Silver, Copper
Copolymers	Block, Graft, Amphiphilic
Electrolytes	Poly, Polymer, Composite, Gel, YSZ
Lithography	Electron Beam, Photo, Nanoimprint, Soft, Optical, Nanosphere, Dip-Pen Nano, Deep Ultraviolet, Interference, Scanning Probe, X-Ray, EUV, AFM, Immersion, Projection, Stereo, Interferometric
Diodes	Light-Emitting, Laser, Photo, Schottky, Barrier, Tunneling, Junction, P-I-N, Wave
Corrosion	Resistance/Protection/Inhibition
Storage	Hydrogen, Charge, Data, Energy, Information, Oxygen, Ion

Table 1.2 (Continued)

Solar Cells	Dye-Sensitized, Photovoltaics, Organic, Silicon, Thin Film, Polymer, Photoelectrochemical, Hybrid, Heterojunction
Transistors	Field-Effect, MOSFETs, Single-Electron, Thin Film, Heterojunction Bipolar, Electron Mobility
Tribology	Wear Resistance/Rate/Mechanisms, Friction Coefficient, Lubrication, Lubricant Films, Solid Lubricants, Scratch Resistance
Detectors	Photo, Infrared, QWIPs, UV
Waveguides	Optical, Ridge, Planar, Photonic Crystal
Etching	Chemical, Reactive Ion, Electrochemical, Dry, Plasma, Wet, Isotropic/Anisotropic, Sputter, ICP, Photo, Silicon, HF, Anodic, Oxide
Batteries	Lithium-Ion
Capacitors	Super, MOS, Electrochemical, MIM, Ferroelectric, Platinum, Film, PZT, Silicon, Double Layer, Embedded
Gate	Dielectrics, Insulators, Stacks
Scaffolds	Tissue Engineering, Composite, PLGA
Chips	Sensor, Bio, Microfluidic
Hard Disk	Drives
Fuel Cells	Oxide, Methanol, Polymer Electrolyte
Circuits	Integrated
Electromechanical Systems	Micro, Nano
Adhesives	Self-Etch, Resins, Conductive, Polyurethane
Piezoelectric	Ceramics, Quartz Crystal
Actuators	Piezoelectric
Recording	Magnetic Media, Optical, Data, Holographic
Cements	Resin, Bone
Molecular Sieves	Mesoporous, Carbon
Memory	Random Access, Nonvolatile Devices, Ferroelectric, Optical, Flash
Transducers	Signal, Ultrasonic
Reactors	Nano, Micro
Field Emitters	Arrays, CNT, Field Emission Gun
Filtration	Gel, Ultra
Displays	Flat Panel, Liquid Crystal
Coatings	Antireflection
Superconductors	Thin Films, Wires
Microlenses	Arrays
Dechlorination/ Generators/ Inductors/ Explosives/ Micromirror/ Quantum/ Computer/ Remote Sensing/ Robotics/ Defluorination/ Optoelectronics/ Switching/ Imprinting/ Screen Printing/ Oxidation Resistance/ Spintronics/ Injection Molding/ Photosensitizers/ Bearings/ Plastics/ Computers/ Resistors/ Micromanipulator	

Nanotechnology has already begun to affect the end products for consumers. Clay nanocomposites are being used to provide an impermeable barrier to gasses such as oxygen or carbon dioxide in lightweight bottles, cartons and packaging films [9]. Storage bins are being produced with silver nanoparticles embedded in the plastic [9]. Making composite fabric with nano-sized particles allows improvement of fabric properties such as waterproofing and stain resistance [11]. A sunscreen based on titanium oxide nanoparticles has a comparable UV protection property as the bulk material [12].

One of the great promises of nanotechnology is the application to biology and medicine. Nanometer-size protein particles called 'self-assembling peptide nanofiber scaffold' were used for the regeneration of axonal tissue of a hamster with severed optic tract [13]. Also it is used for site-specific or targeted drug delivery applications. Nanoparticles selectively coated with biodegradable polymer can carry the drug *in vivo* to the desired location such as tumor cells or around inflammation sites as the polymer degrades [14]. Superparamagnetic magnetite particles coated with dextran are used as image enhancement agents to detect small lymph-node metastases of prostate cancer in magnetic resonance imaging [15]. Certain nanoparticles integrated on chips, 'Lab-on-a-chip', to work as tags or labels are used as biological tests measuring the presence or activity of selected substances become quicker, more sensitive and more flexible [16].

Applying nanotechnology to electronics has led that the smallest feature of a transistor shrunk from 10 μm down to 30 nm during the past four decades [17].

Nanotechnology is also used for the environmental studies. The chemical reactivity of magnetic nanoparticles can be functionalize by the surface coatings and can be used chemical separation or chemical decomposition applications against the pollutants in water since they have high surface areas and give response to a magnet or a magnetic field [18].

Nanotechnology plays a role for increasing the efficiency of energy production by using more environmental-friendly energy systems such as fuel cells and nano-batteries. Multi-walled nanotubes filled with nanowires of Ni/ternary Zr based hydrogen storage alloy have been studied for the development of such systems [19].

1.2 Nanoparticles

Buzea et al. described the nanoparticles as the particles with at least one dimension smaller than 1 μm [11]. According to International American Society for Testing and Materials (ASTM), a particle ranging in size from approximately 0.1 μm (100 nm) to 0.001 μm (1 nm) belongs to the ultrafine particle category. Nanoparticle is defined as the sub-classification of ultrafine particle with lengths in two or three dimensions greater than 1 nm and smaller than about 100 nm and may or may not exhibit a size-related intensive property [20].

Nanoparticles can be in form of amorphous or crystalline. Buzea et al. proposed that in addition to the solid, liquid, gaseous, and plasma states of matter, nanoparticulate should be considered a distinct state of matter to some degree because of its properties such as large surface area and quantum size effects [11].

The properties of materials change as their size approaches the nanoscale and as the percentage of atoms at the surface of a material becomes significant. These affect the mechanical, optical, electrical, magnetic properties and chemical reactivity such as quantum confinement in semiconductor particles, surface plasmon resonance in some metal particles and superparamagnetism in magnetic materials.

The nanoparticles have a very large surface area compared to the bulk. For example, the ratio of the surface area of a cube with a side length of 1 cm is 10,000 times smaller than a cube with a side length of 1 μm as illustrated at Figure 1.1. Subsequently, dividing the cube of 1 μm into a cube of 10 nm increases the specific surface area by 100 fold [21]. The chemical reactivity and the reaction rates of the

particles increase as the specific surface area increases inversely proportional with the particle size [11].

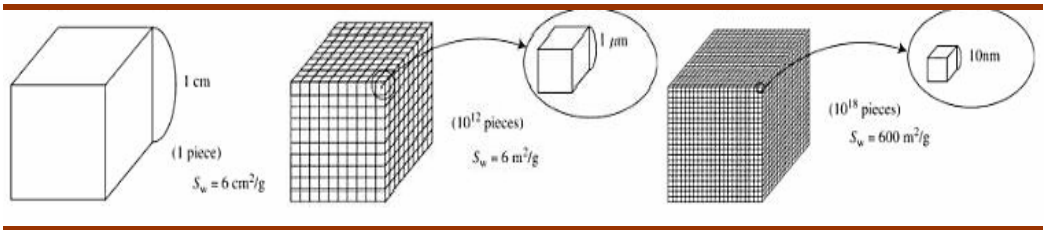

Figure 1.1 Change of specific surface area [21]

The decrease in the particle size leads activation on the particle surface. Since the atoms situated at the surface of a nanoparticle have fewer neighbours than bulk atoms, they are more active which leads to easy bonding with the contacting materials. Because of this lower coordination, surface atoms are less stabilized than bulk atoms and have the higher the average binding energy per atom [22].

When the particle size decreases to nanometer size, magnetic materials exhibit unique properties such as superparamagnetism that can not be seen in their bulk forms. In a bulk ferromagnetic material, the magnetization M is the vector sum of all the magnetic moments of the atoms in the material per unit volume of the material. The bulk material consists of domains with each domain having its own magnetization vector arising from an alignment of atomic magnetic moments within the domain. The magnetization vectors of all the domains in the material may not be aligned, leading to a decrease in the overall magnetization. When the length scale of the material becomes small, however, the number of domains decreases until there is a single domain when the characteristic size of the material is below some critical size d_C [29].

Franks has summarized the preparation methods of nanoparticles under six topics. These are sol-gel processes, solid-state reactions, liquid-solid reactions, evaporation

and condensation processes, plasma processes, and flame hydrolysis. Among these, liquid-solid reactions was defined as precipitation from a solution in which the process being dependent on the presence of the desired nuclei [23].

1.2.1 Iron Oxide Nanoparticles

Due to the unique properties like superparamagnetism, high coercivity, low Curie temperature and high magnetic susceptibility, magnetic iron oxide nanoparticles have a great importance for the researchers in a broad range of disciplines, including magnetic fluids, data storage and catalysis to bioapplications [24]. Especially, iron oxide nanoparticles with appropriate surface chemistry have numerous *in vivo* applications in biomedical area such as magnetic resonance imaging (MRI) [14], the deterioration of cancer cells via hyperthermia treatment [15], tissue repair, immunoassay, detoxification of biological fluids, drug delivery, and cell separation. At this sense, an accurate choice of the nanomaterial with adjustable physical and chemical properties plays an important role for such kinds of applications shown in Figure 1.2. In this consideration, magnetic iron oxide nanoparticles became the strong candidates [24].

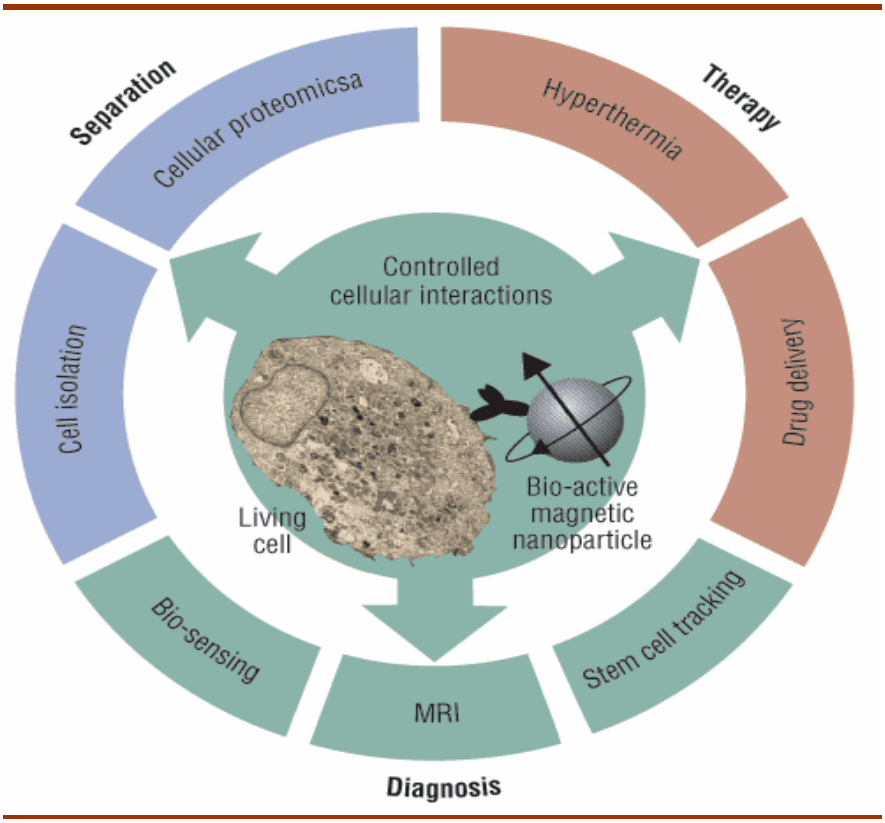

Figure 1.2 Biomedical applications of biologically activated magnetic nanoparticles [25]

The 1-100 nm sized iron oxide nanoparticles show properties superior than traditional micrometer sized particles. Among the advantages these particles promote the users, they have high surface to volume atoms ratio. Moreover, sufficiently small magnetic nanoparticles show superparamagnetic behaviour [26]. The unique combination of high magnetization and paramagnetic behaviour opens these materials to a very wide range of applications. Also, the possibility of surface modifications with biologically active compounds increases the popularity of these particles [27]. The requirements for high performance of these nanoparticles are having particle size lower than 100 nm, a narrow size distribution and of course, high magnetization values [28].

1.2.2 The Magnetic Properties of Iron Oxide Nanoparticles

The iron atom has a strong magnetic moment. The reason for this is due to four unpaired electrons in its 3d orbitals. Different magnetic cases are occurred when the crystals are formed from the iron atoms [29]. The details of the iron oxides magnetism conditions are given below and shown in Figure 1.3.

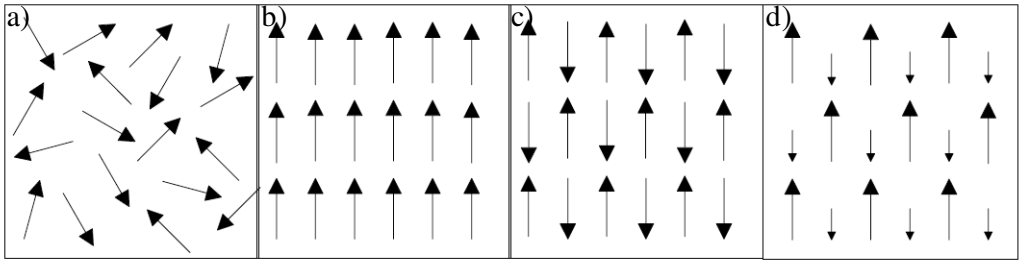

Figure 1.3 Different orientations of magnetic dipoles: (a) paramagnetic (b) ferromagnetic (c) antiferromagnetic and (d) ferrimagnetic

1.2.2.1 Paramagnetism

In the paramagnetic state, the individual atomic magnetic moments are randomly aligned with respect to each other, and the crystal has a zero net magnetic moment. If an external magnetic field is applied to the crystal, some of these moments will align and the crystal will attain a small net magnetic moment [29].

1.2.2.2 Ferrimagnetism

Ferrimagnetic substances like antiferromagnetic materials has at least two interpenetrating sublattices and the alignment of spins is antiparallel. However, in

this type of magnetic materials spins have not equal moments which results in ferrimagnetic material having a net magnetic moment [30].

1.2.2.3 Ferromagnetism

In a ferromagnetic crystal, all the individual atomic magnetic moments are aligned even without an external field. On the other hand, ferrimagnetic crystal has a net magnetic moment from two types of atoms with moments of different strengths that are arranged in an antiparallel order [29].

1.2.2.4 Antiferromagnetism

The crystal is called antiferromagnetic, showing no net magnetic moment, if the antiparallel magnetic moments are of the same magnitude [29].

1.2.2.5 Superparamagnetism

A superparamagnetic material is a single domain magnetic material which has no hysteresis loop. Iron oxide nanoparticles having size smaller than 20 nm shows generally superparamagnetic behaviour at room temperature [30].

Due to thermal fluctuations of the individual moments, the ordered arrangement of magnetic moments decreases with increasing temperature. The material becomes disordered and loses its magnetization beyond the Ne´el or Curie temperature [29].

1.2.2.6 Hysteresis Loop

One of the important issues to be considered when discussing magnetic materials is the shape of the hysteresis loop. When a material is magnetized in one direction, it will not relax back to zero magnetization when the imposed magnetizing field is

removed. It must be driven back to zero by a field in the opposite direction. If an alternating magnetic field is applied to the material, its magnetization will trace out a loop called a hysteresis loop [30]. A hysteresis loop shows the relationship between the induced magnetic flux density (**B**) and the magnetizing force **(H).** It is often referred to as the B-H loop and shown in Figure 1.4.

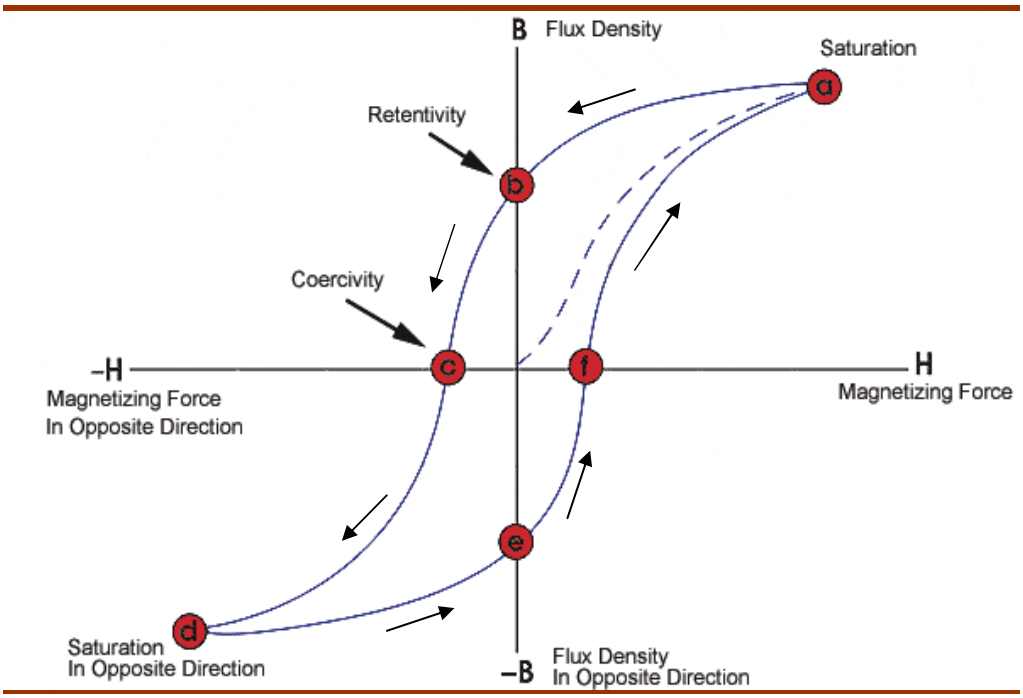

Figure 1.4 Hysteresis loop [31]

i. *Point 'a'*: This point is where nearly all magnetic domains are in the same order and hence, the maximum magnetic saturation the material can ever reach. Here, in the case of an additional increase in magnetizing force, there will be only a little increase in the magnetic field.

ii. *Point 'b'*: The transform from point 'a' to the point 'b' is occurred when *H* is decreased to zero. At this point, the magnetizing force is zero but nevertheless, there is still some magnetic flux kept by the material. This point is also at where one

should look for *retentivity* on the graph, showing and indicates the level of magnetism retained in the material.

iii. *Point 'c'*: At this point, the magnetizing force is reversed leading to a decrease in flux down to zero. This is also the *coercivity* point.

iv. *Point 'd'*: Here, there is a negatively increase in the magnetizing force and hence, the material again reaches the maximum saturation in magnetization in opposite direction.

v. *Point 'e'*: *H* is decreased down to zero at this point. The magnetism retained in the material at this stage is also equal to one at the point *b* with the opposite direction.

vi. *Point* 'f': With a positive increase in *H*, *B* is reduced to zero. This is what called as *f* point. From here, the curve goes through the maximum saturation point (*a*) and by this way, makes a complete loop [32].

Using the hysteresis loop, one can get some specific information about magnetic properties of materials, such as retentivity, coercive force, residual magnetism, permeability and reluctance. There is a strong relationship between the retentivity and residual magnetism. *Retentivity* is a concept standing for the ability of the material to keep a certain amount of magnetic field in the case of the removal of the magnetic field after the saturation whereas *residual magnetism* means the flux density retaining in the material in zero magnetizing force. At the saturation point, these two terms are same. However, at a level of lower than the saturation point, residual magnetism may be also lower than the related retentivity value. On the other hand, *coercive force* term is used to express the amount of needed magnetic field to be applied reversely to decrease down the flux to zero and *permeability,* denoted as μ, describes the ease of the establishment of the magnetic flux in the component. Additionally, *reluctance* works like resistance in an electrical circuit and is the opposition of the ferromagnetic material to the magnetic field [32].

Although there are numerous types of iron oxide compounds in nature, γ-Fe_2O_3 as maghemite, α-Fe_2O_3 as hematite and Fe_3O_4 as magnetite are among well-known iron

oxide crystallines [29]. The physical and chemical properties of iron oxides are summarized in Table 1.3.

Table 1.3 Physical and chemical properties of iron oxides [30]

Name of the iron oxide phase	Hematite	Magnetite	Maghemite
Molecular Formula	α-Fe_2O_3	Fe_3O_4	γ-Fe_2O
Density (g/cm^3)	5.26	5.18	4.87
Melting Point (^oC)	1350	1583-1597	---
Hardness	6.5	5.5	5
Type of Magnetism	Weakly ferromagnetic or antiferromagnetic	Ferrimagnetic	Ferrimagnetic
Curie Temperature (K)	956	850	820-986
M_S at 300 K ($A\ m^2/kg$)	0.3	92-100	60-80
Standard Free Energy of formation ΔG_f° (kJ/mol)	-742.7	-1012.6	-711.1
Crystallographic System	Hexagonal (rhombohedral)	Cubic	Cubic or tetrahedral
Structural Type	Corundum	Inverse spinel	Defect spinel
Space Group	R3c (hexagonal)	Fd3m	$P4_332$ (cubic); $P4_12_12$ (tetragonal)
Lattice Prameter (nm)	a=0.5034, c=1.375 (hexagonal) a_{Rh}=0.5427, α=55.3^o (rhombohedral)	a=0.8396	a=0.83474 (cubic); a=0.8347, c=2.501 (tetragonal)

1.2.3 Magnetite

Magnetite (Fe_3O_4) is a common magnetic iron oxide nanoparticle shown in Figure 1.5 and also known as black iron oxide, magnetic iron ore, loadstone, ferrous ferrite, or Hercules stone. Among the transition metal oxides, it exhibits the strongest magnetism [29].

Figure 1.5 Magnetite ore [33]

Due to its typical magnetic and electrical properties, magnetite is one of the preferred and widely used in numerous industrial processes (*e.g.*, printing ink), environmental applications (*e.g.*, magnetite carrier precipitation processes for metal ion removal and magnetic filtration) and also medical applications (biomolecule separation and contrast agents for NMR imaging), some of which are really exciting and are under development at the moment (drug targeting and hyperthermia) [34].

The synthesis of magnetite nanoparticles can be performed by several methods, such as polyol process, precipitation route, sonochemical synthesis and microemulsion technique [35].

To talk about the structural properties of magnetite, it has a cubic inverse spinel structure as shown in Figure 1.6. Here, oxygen anions form a FCC closed packing and Fe cations occupying the interstitial tetrahedral sites and octahedral sites. The electrons can hop between Fe^{2+} and Fe^{3+} ions in the octahedral sites at room temperature, rendering magnetite an important part of half-metallic materials [36] It has an Fd3m point group and the lattice constant of a=0.8396 [29].

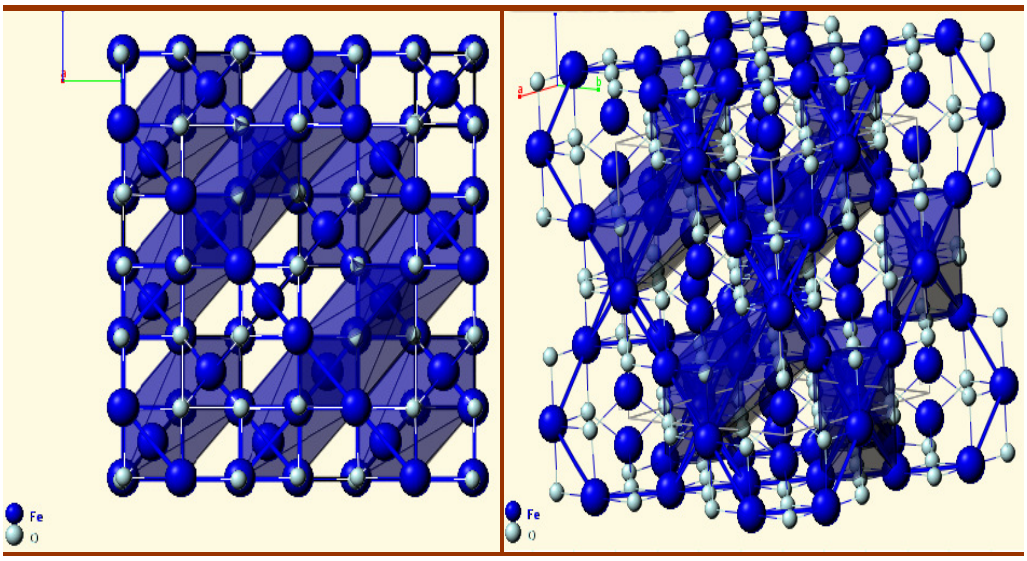

Figure 1.6 Crystal structure of magnetite [33]

Magnetite is ferrimagnetic at room temperature and has a Curie temperature, T_C of 850 K. It has a rather high Curie temperature when compared to other phases of iron oxide. It is a mixed valence compound. Ferric ions fully occupy the tetrahedral (A) sublattices. Half of the octahedral (B) sublattices are occupied by Fe^{2+} ions and other half are occupied by Fe^{3+} ions. Below T_C, A-site magnetic moments are aligned antiparallel to the B-site magnetic moments. The net effect is that the magnetic contributions of both sites are not balanced and there is a permanent magnetism [37].

1.2.4 Maghemite

Maghemite (γ-Fe_2O_3) is one of the magnetic forms of iron oxides and has a brown color as shown in Figure 1.7. Due to its nontoxicity, biocompatibility, biodegradability, low particle dimension, large surface area and suitable magnetic properties, its application area is great wide varying from biomedical and biological applications including magnetic resonance imaging (MRI) contrast enhancement, biomagnetic separations, hyperthermia treatment to magnetic drug targeting [38].

Figure 1.7 Maghemite ore [33]

To prepare maghemite nanoparticles, there are numerous ways such as co-precipitation, microemulsions, high temperature decomposition of organic precursors and oxidization of magnetite nanoparticles [39]. Additionally, in industry, these nanoparticles are prepared by thermal dehydration of goethite to hematite, followed by partial reduction to magnetite and re-oxidation to maghemite [40].

Maghemite has spinel structure with a difference of vacancies in the cation sublattice as shown in Figure 1.8. It has cubic or tetrahedral crystal system. For cubic

maghemite nanoparticles, the point group symmetry is $P4_332$ and the characteristic lattice parameter is a=0.83474. In the case of tetragonal maghemite particles, the point group symmetry is $P4_12_12$ with lattice parameters of a=0.8347, and c=2.501 [29].

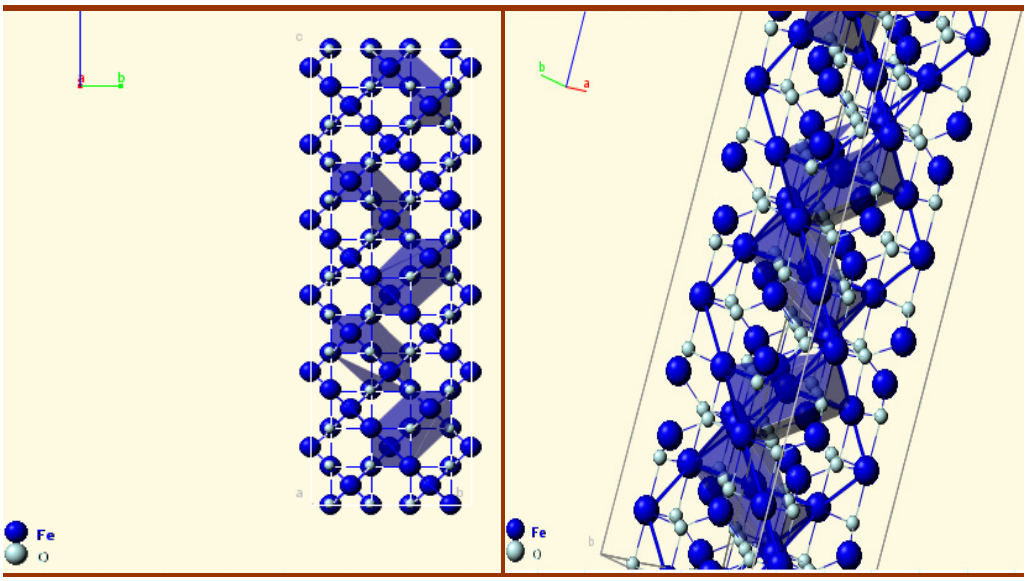

Figure 1.8 Crystal structure of maghemite [33]

1.3 The Zeta Potential

The electric potential difference which is occurring at the boundary between the mobile phase and the stationary layer of immobile phase is called the zeta potential. The isoelectric point is the pH at which the situation corresponds to net zero effective charge at the surface [41].

Zeta potential is calculated from the measured particle electrophoretic mobility (μ_e) by using the Smoluchowski equation (Eq. [1.1]):

$$\zeta = \frac{\eta}{\epsilon} \mu_e \qquad [1.1]$$

where η is the viscosity and ϵ is the dielectric constant of the dispersion medium [42].

Surface charge has a critical influence on obtaining stable nanoparticles so the dispersion will resist aggregation. In other words, to prevent nanoparticles from agglomeration and confer stability, zeta potential of the medium should be adjusted carefully. Theoretically, zeta potential larger than ±30 mV is an ideal value to keep iron oxide nanoparticles stable [43].

1.4 Sonochemistry

Sonochemistry is defined as chemical reactions driven by sound or ultrasound, usually through the process of acoustic cavitation in a liquid, liquid slurry, or at a liquid-solid/gas interface. Sonochemistry has been employed to dramatically increase reaction rates of mixed-phase reactions (especially liquid-solid reactions of reactive metals), to synthesize nanostructured inorganic materials [44].

The chemical consequences of high-intensity ultrasound do not arise from an interaction of acoustic waves and matter at a molecular or atomic level. Instead, the primary mechanism for sonochemical effects in liquids irradiated with high-intensity ultrasound is the acoustic cavitation. It can be defined as the formation, growth, oscillation, and collapse of bubbles in a liquid [44].

The bubble formed because of acoustic cavitation grows and then collapses. During this collapses of bubbles, intense local heating, high pressures are produced in very short lifetimes. High-energy chemical reactions occur at these temporary, localized hot spots. These hot spots have temperatures of ~5000°C, pressures of about 1000

atm, and heating and cooling rates above 10^{10} K/s. Hence, the diffuse energy of sound is concentrated into a unique set of conditions by means of cavitation [45].

In liquid-solid systems, non-spherical bubble collapse near a solid surface drives high-speed jets of liquid into the surface and creates shockwave damage to the surface as represented in Figure 1.9. The most of the available energy is transferred to the accelerating jet, rather than the bubble wall itself so this jet can reach velocities of hundreds of meters per second. In addition, shockwaves created by cavity collapse in the liquid may also induce surface damage and the fragmentation of brittle materials. The impingement of microjets and shockwaves on the surface creates the localized erosion responsible for many of the sonochemical effects on heterogeneous reactions. In brief, ultrasonic cavitation in liquid-solid systems gives rise to the physical effects primarily responsible for such enhancements include (a) improvement of mass transport from turbulent mixing and acoustic streaming, (b) the generation of surface damage at liquid-solid interfaces by shock waves and microjets, (c) the generation of high-velocity interparticle collisions in slurries, and (d) the fragmentation of friable solids to increase surface area [45].

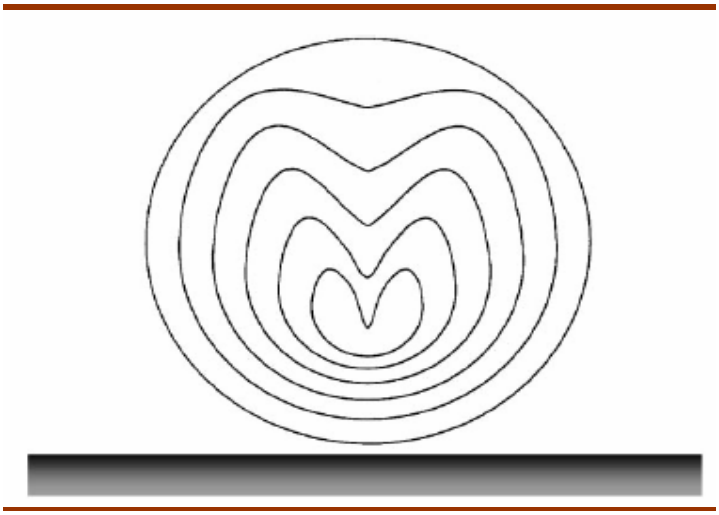

Figure 1.9 Formation of a liquid microjet during bubble collapse near an extended surface [45]

1.5 Recent Literature Survey

There are various routes for the synthesis of magnetic nanoparticles. The most used ones are microemulsion [26,46], laser pyrolysis [29], sol-gel method [29,36], hydrothermal synthesis [47], chemical vapour condensation [48,49], thermal decomposition [50] and co-precipitation [51,52].

Among these, one of the important and commonly used method to synthesize nanoparticles is the sol-gel method [53]. In this procedure, sol-gel is synthesized in the liquid media. The sol means a solution of solid particles in a liquid. Hydrolysis and condensation of molecular precursors yield a solid structure swollen with liquid which is called gel [54]. Iron oxide nanoparticles within the range of 5-100 nm were synthesized [55-57]. The sol-gel method has been shown to be very useful for the preparation of γ-Fe_2O_3 nanoparticles. By this method, maghemite nanoparticles can be embedded in an inert, inorganic, transparent and temperature resistant silica matrix. Factors such as the nature and concentration of the iron salt precursor employed, the surface of evaporation/volume ratio of the sol and the temperature of the following heat treatments have been shown to have an important influence on the particle size, the size distribution and the iron oxide phase in the final composite [57-60]. In addition, unique magnetic properties had been investigated for the iron oxide particles embedded on sol-gel matrix [61-63].

Another common and important method for the production of nanoparticles is the co-precipitation method [64,65]. It is a simple and inexpensive method depending on forming spherical iron oxide particles from aqueous Fe^{2+}/Fe^{3+} salt solutions by the addition of a base under inert atmosphere at room temperature or at elevated temperature [66]. The size, shape, and composition of the magnetic nanoparticles very much depends on the type of salts used (e.g. chlorides, sulfates, nitrates), the Fe^{2+}/Fe^{3+} ratio, the reaction temperature, the pH value and ionic strength of the media [67-71]. It has been shown that spherical magnetite particles with mean diameters ranging from 30 to 100 nm can be obtained by the reaction of a Fe(II) salt,

a base and a mild oxidant (nitrate ions) in aqueous solutions [72]. Stoichiometric mixtures of ferrous and ferric hydroxides can also be reacted in aqueous media to yield homogeneous spherical particles of either magnetite or maghemite [73]. Due to the large surface-area to volume ratio, nanoparticles formed by liquid phase co-precipitation tend to aggregate in solution in order to reduce their surface energy [29].

Because of the tendency of aggregation, ease of transformation of magnetite nanoparticles to other iron oxide phases, maintaining the stability and protection of the magnetite particle is a must. To accomplish this, polymer coating is used to improve the chemical stability and dispersibility of the Fe_3O_4 nanoparticles. In addition, with polymer coating, the functionalization of the surface is obtained. Surface-modified magnetic nanoparticles with certain biocompatible polymers are intensively studied for magnetic-field-directed drug targeting, and as contrast agents for magnetic resonance imaging [14,15]. Polymers containing functional groups, such as carboxylic acids, phosphates, and sulfates, can bind to the surface of magnetite [30]. Suitable polymers for coating include polystyrene [74], poly(3, 4-ethylenedioxythiophene) [75], polymethyl methacrylate [76], poly(ethylene glycol) [77], poly(methacrylic acid) [78], poly(pyrrole) [79], poly(aniline) [80], poly(alkylcyanoacrylates) [81], and polyesters, such as poly(lactic acid), poly (glycolic acid), poly(e-caprolactone), and their copolymers [82]. The common way of polymer coating is to synthesize the magnetic nanoparticle separately and subsequently to coat the particles by either polymerization from monomer or chemical or physical adsorption onto the magnetic particles [83]. The particle size range of polymer coated nanoparticles reported in literature varies from 0.27 μm to 2.8 μm [84-87].

While synthesizing polymer coated nanoparticles, applying ultrasound irradiation is a useful method in order to control the primary particle size and to obtain monodisperse smaller particles in matrix and relatively thinner polymer coatings. In the literature, this method was used many times and primary particles between 5 and 20 nm were obtained [88-89]. The use of ultrasonic irradiation for the polymer

coating methods such as miniemulsion or *in situ* polymerization results in easy and efficient surface coating of the smaller particles, which is important for biological applications [83-90].

1.6 Aim of the Study

In this study, two different iron oxide nanoparticles; maghemite (γ-Fe_2O_3) and magnetite (Fe_3O_4) will be prepared in two different matrixes; sol-gel and p poly(methacrylic acid), respectively. In the preparation of maghemite nanoparticles in sol-gel matrix, the effect of the factors such as the type of the iron salt, evaporation rate, calcination temperature on the iron oxide phase and primary nanoparticle size will be investigated. Magnetite (Fe_3O_4) nanoparticles were synthesized via co-precipitation in aqueous solution under ultrasonic irradiation. The effect of ultrasonic agitation on the surface and volume weighted mean sizes and specific surface area of PMAA-coated magnetic agglomerates during sample preparation will be investigated and compared with the use of conventional magnetic stirring. The aim was to decrease the size of the agglomerates and increase the specific surface area.

The crystal structure of iron oxide particles and the primary particle size will be determined by X-ray diffraction. The polymer coated Fe_3O_4 nanoparticles will be characterized using field emission scanning electron microscopy (FE-SEM). The agglomerate size of PMAA coated magnetite nanoparticles will be measured using laser particle sizer. The zeta potential measurements will be done to investigate the colloidal stability and the presence of the PMAA on the surface. In order to measure the magnetic properties, vibrating sample magnetometer (VSM) will be used.

CHAPTER 2

EXPERIMENTAL

2.1 Chemicals and Reagents

2.1.1 Synthesis of γ-Fe_2O_3 Nanoparticles in Sol-Gel Matrix

i. Tetraethyl orthosilicate, TEOS ($Si(OC_2H_5)_4$), 99%: Aldrich, named also as tetraethoxysilane

ii. Iron(III) nitrate nonahydrate, ($Fe(NO_3)_3.9H_2O$), 99%: Fluka, named also as ferric nitrate nonahydrate

iii. Iron (III) chloride hexahydrate, ($FeCl_3.6H_2O$), 97%: Aldrich, named also as ferric trichloride hexahydrate

iv. Ethanol, (CH_3CH_2OH), 99.5%: Sigma-Aldrich; named also as ethyl alcohol

2.1.2 Synthesis of PMAA-Coated Fe_3O_4 Nanoparticles

i. Ferrous sulfate heptahydrate ($FeSO_4.7H_2O$), 99%: AnalaR by British Drug Houses, named also as iron (II) sulfate heptahydrate

ii. Iron (III) chloride hexahydrate ($FeCl_3.6H_2O$), 97%: Aldrich, named also as ferric trichloride hexahydrate

iii. Poly(methacrylic acid, sodium salt), (PMAA), 30 wt % solution in water: Aldrich, Typical M_n= 5400, Typical M_w= 9500

iv. Hydrochloric acid (HCl), 37%: Merck

v. Sodium hydroxide pellets (NaOH): Riedel-de Haën

vi. Nitrogen gas (N_2), pure: Habaş Sınai ve Tıbbi Gazlar İstihsal Endüstrisi A.Ş.

Deionized water was obtained from Millipore water purification system. Nitrogen gas was passed through deionized water for forty minutes in order to achieve deoxygenated water. It was used for all sample preparations and washing procedures.

0.01 M HCl solution was prepared from diluting hydrochloric acid (37%, Merck) with deoxygenated water. It was used for washing procedures.

All the glass and plastic wares were cleaned by soaking in 10% HNO_3 for at least for 24 hours and then rinsed three times with distilled water and then with deionized water.

All the chemical reagents, solutions and samples were handled with appropriate safety precautions to avoid personal damage and corrosion of the equipment.

2.2 Instrumentation

2.2.1 High Intensity Ultrasonic Liquid Processor

Sonics VCX series 500 Watt ultrasonic processor with sound abating enclosure (Figure 2.1) was used during the synthesis of PMAA coated magnetite nanoparticles. A titanium alloy standard probe with threaded end and replaceable tip was employed

during the synthesis. A stainless steel temperature probe integrated to the ultrasonic processor allowed to control the sample temperature up to 100^{o}C.

Figure 2.1 Ultrasonic processor with sound abating enclosure during the synthesis

The operation conditions of ultrasonic processor used during the synthesis were summarized in Table 2.1. Unless stated otherwise, the conditions given in Table 2.1 were used throughout the experiments.

Table 2.1 Instrumental parameters used for the synthesis of PMAA coated magnetite nanoparticles

Ultrasonication Time	40 minutes
Maximum Limit of Temperature for Reaction Medium	30°C
Pulse of Ultrasonic Irradiation	10 seconds ON / 10 Seconds OFF
Amplitude of Ultrasonic Irradiation	40%
Energy	___

2.3 Procedure

2.3.1 Synthesis of Maghemite (γ-Fe_2O_3) Nanoparticles in Sol-Gel Matrix

For the sol-gel method a series of iron oxide/silica nanocomposites with Fe/Si molar ratio of 0.25 were prepared by adding 5 ml of tetraethylorthosilicate (TEOS) to an initial solution which was obtained by dissolving iron (III) nitrate, ($Fe(NO_3)_3.9H_2O$) or iron (III) chloride hexahydrate, ($FeCl_3.6H_2O$) into 15 ml and 22.5 ml of ethanol. The sample contained 25 wt % $Fe_2O_3/(Fe_2O_3+SiO_2)$. The hydrolysis reaction was promoted only by the hydration water of the salt. After stirring for 1 hour at room temperature, clear sols having approximately a pH value of 1 were obtained. The sols were poured into identical glass vessels. The surface/volume (S/V) ratios which were

calculated by dividing the evaporation surface (the cross-section of the vessel) by the volume of the sol (Figure 2.2) were taken 0.03 and 0.04.

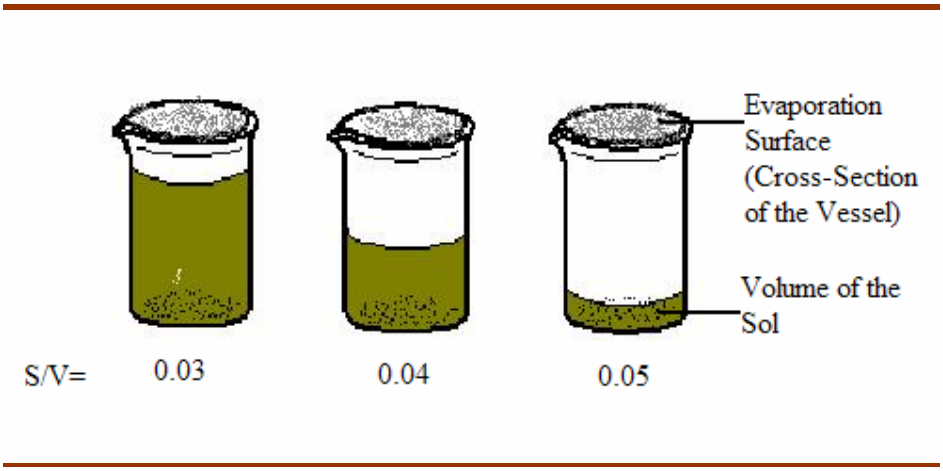

Figure 2.2 Surface to volume ratio (S/V)

The vessels were closed using a seal with a small punched hole and the sols were allowed to gel in an oven at 50 °C for 15 days. Further, they were kept at 150 °C for 24 h for the elimination of residual water. Finally, the samples were treated at a higher temperature, with steps of 50 °C from 150 °C up to 500 °C, kept for 30 min at each temperature and up to 900 °C with steps of 100°C, kept for one hour at each temperature. Some of the samples were only heated to 400 °C for 4 h in air to observe the effect of heat treatment temperature on the phases produced in the Fe_2O_3-SiO_2 nanocomposite.

2.3.2 Synthesis of Poly(methacrylic acid)-Coated Magnetite (Fe_3O_4) Nanoparticles

Two different procedures were investigated for the synthesis of PMAA-coated magnetite nanoparticles. PMAA coated magnetite particles were prepared either *ex situ*, that is, the Fe_3O_4 nanoparticles were prepared first and then subjected to the

PMAA solution under magnetic stirring or ultrasonic agitation or *in situ* where the iron oxide nanoparticles were synthesized in the presence of PMAA.

2.3.2.1 Synthesis of Magnetite Nanoparticles under Ultrasonic Agitation

At this procedure, Fe_3O_4 nanoparticles were synthesized with ultrasonication. Initially the precursor solution was prepared by diluting a mixture of $1.7x10^{-3}$ moles of $FeSO_4.7H_2O$ and $3.4x10^{-3}$ moles of $FeCl_3.6H_2O$, 2.5 ml 12.06 M HCl to 50 ml with deoxygenated water. The molar ratio of Fe^{2+}/Fe^{3+} was 1:2. The precursor solution was always mixed under magnetic stirring during the addition of iron salts and acid and nitrogen gas was passed through the vessel during the mixing. After dissolution of iron salts, 18.75 ml of the precursor solution was added dropwise by a help of burette to 187.5 ml of 1.5 M NaOH solution prepared with deoxygenated water under ultrasonic irradiation. Nitrogen gas was passed through the reaction vessel during the ultrasonication. The experimental set-up can be observed at Figure 2.3 and Figure 2.4. The experimental conditions which were summarized at Table 2.1 were applied.

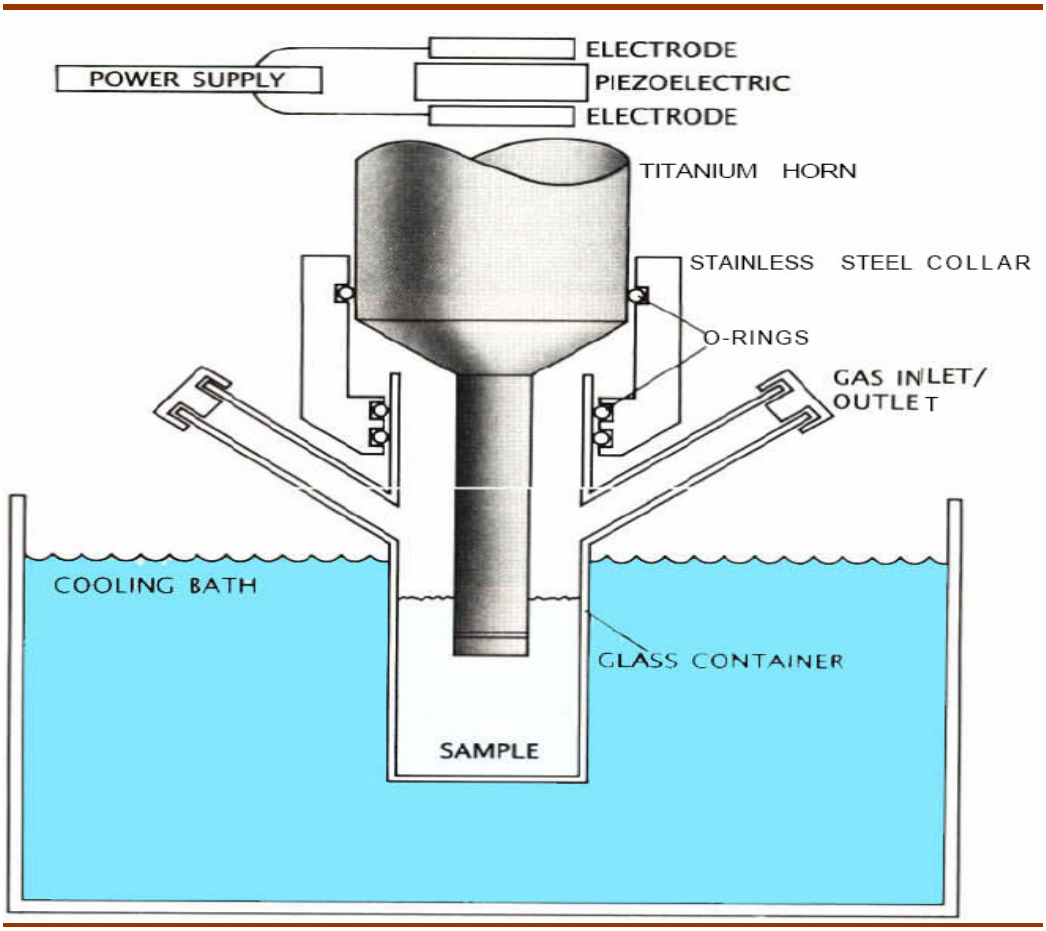

Figure 2.3 Schematic diagram of conventional high intensity ultrasonic liquid processor experimental set-up

After ultrasonication, the black solution was centrifuged at 4000 rev/min for 5 minutes. After isolating the black solid, the supernatant was decanted. The black product, claimed to be magnetite nanoparticles, was washed using deoxygenated water five times and centrifuged at 8000 rev/min for the first washing cycle, at 10000 rev/min for the subsequent two washing cycles and then at 13,500 rev/min for the last two washing cycles. The black product was finally washed with 0.01 M HCl and centrifuged at 13500 rev/min. The resulting Fe_3O_4 nanoparticles were dispersed in deoxygenated water and final pH was adjusted to 3 with 0.01 M HCl. The sample was named as S1.

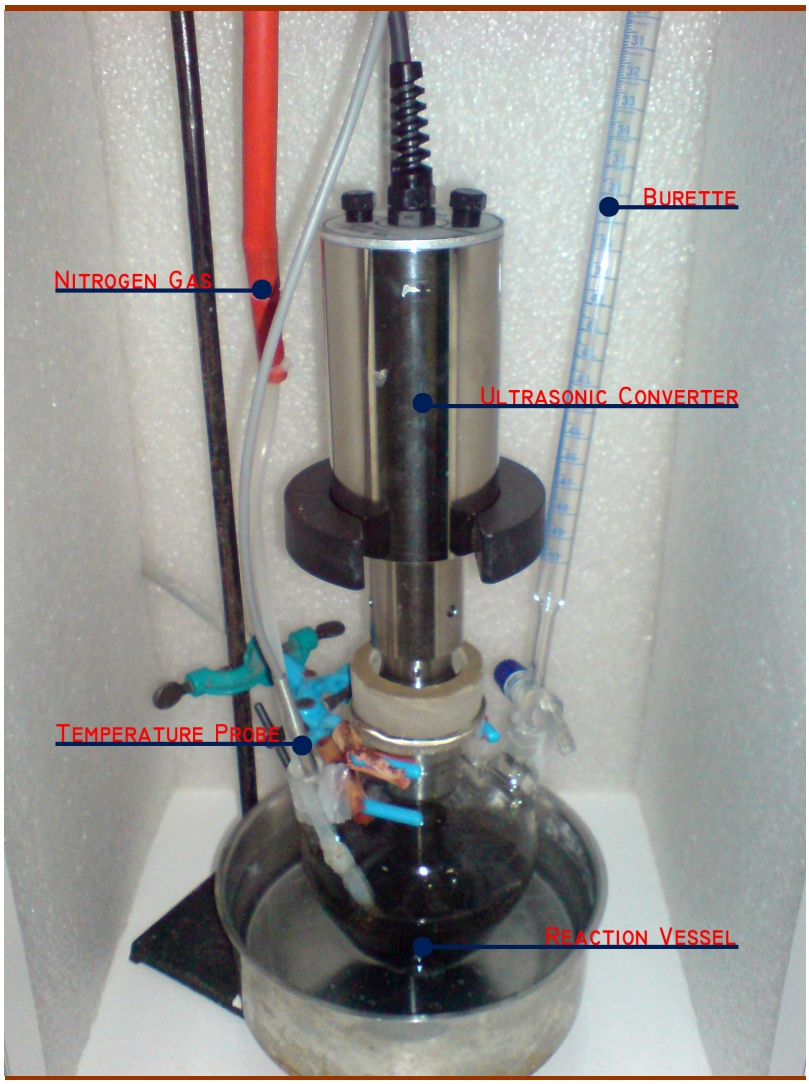

Figure 2.4 Experimental set-up

2.3.2.2 *Ex Situ* Synthesis of PMAA-coated Magnetite Nanoparticles, Two-step Procedure

In order to accomplish the *ex situ* synthesis of PMAA-coated Fe_3O_4 nanoparticles, two-step procedure was applied. Initially, magnetite nanoparticles were prepared under ultrasonic agitation. Then, these freshly prepared Fe_3O_4 nanoparticles were

subjected to two different routes for PMAA-coating. The first one was coating under magnetic stirring and the second one is coating under ultrasonic agitation.

2.3.2.2.1 *Ex Situ* Synthesis of PMAA Coated Magnetite Nanoparticles under Magnetic Stirring

In magnetic stirring procedure, the polymer coating of the nanoparticles was realized under magnetic stirring after the synthesis of the Fe_3O_4 nanoparticles. At this procedure, initially Fe_3O_4 nanoparticles were prepared under ultrasonic irradiation with the same way described in Section 2.3.2.1.

Subsequently, in a two-necked round bottom flask, 7 ml poly(methacrylic acid) (PMAA) and 2.5 ml 12.06 M HCl were mixed and diluted to 50 ml with deoxygenated water under magnetic stirring. Nitrogen gas was passed through the vessel during mixing. This solution was named as PMAA solution.

An aliquot of PMAA solution was added dropwise by a help of a burette to 9 mM Fe_3O_4 nanoparticles solution under vigorous magnetic stirring. The resulting mixture was mixed for 40 minutes in order to coat the Fe_3O_4 nanoparticles efficiently. Nitrogen gas was passed through the reaction vessel during the mixing.

After mixing, the black solution was centrifuged at 4000 rev/min for 5 minutes. After isolating the black solid, the supernatant was decanted. The black product, claimed to be PMAA-coated magnetite nanoparticles was washed using deoxygenated water five times and centrifuged at 8000 rev/min for the first washing cycle, at 10000 rev/min for the subsequent two washing cycles and then at 13,500 rev/min for the last two washing cycles. The black product was finally washed with 0.01 M HCl and centrifuged at 13500 rev/min. The resulting PMAA-coated Fe_3O_4 nanoparticles were dispersed in deoxygenated water and final pH was adjusted to 3.5 with 0.01 M HCl. The sample was named as S2.

2.3.2.2.2 *Ex Situ* Synthesis of PMAA Coated Magnetite Nanoparticles under Ultrasonic Agitation

In ultrasonication procedure, the polymer coating of the nanoparticles was realized with ultrasonic irradiation after the synthesis of the Fe_3O_4 nanoparticles. At this procedure, initially Fe_3O_4 nanoparticles were prepared under ultrasonic irradiation with the same way described in Section 2.3.2.1.

In a separate flask, 7 ml poly(methacrylic acid) (PMAA) and 2.5 ml 12.06 M HCl were mixed and diluted to 50 ml with deoxygenated water under magnetic stirring. Nitrogen gas was passed through the vessel during mixing. This solution was named as PMAA solution.

An aliquot of PMAA solution was added dropwise by a help of a burette to initially synthesized 9 mM Fe_3O_4 nanoparticles solution under ultrasonication. The experimental set-up, which can be observed at Figure 2.4, was used and the experimental conditions which were summarized at Table 2.1 were applied. Nitrogen gas was passed through the reaction vessel during ultrasonication.

After mixing, the black solution was centrifuged at 4000 rev/min for 5 minutes. After isolating the black solid, the supernatant was decanted. The black product, claimed to be PMAA-coated magnetite nanoparticles was washed using deoxygenated water five times and centrifuged at 8000 rev/min for the first washing cycle, at 10000 rev/min for the subsequent two washing cycles and then at 13500 rev/min for the last two washing cycles. The black product was finally washed with 0.01 M HCl and centrifuged at 13500 rev/min. The resulting PMAA-coated Fe_3O_4 nanoparticles were dispersed in deoxygenated water and final pH was adjusted to 3.5 with 0.01 M HCl. The sample was named as S3.

2.3.2.3 *In Situ* Synthesis of PMAA Coated Magnetite Nanoparticles, One-Step Procedure

The precursor solution was prepared by diluting a mixture of $1.7x10^{-3}$ moles of $FeSO_4.7H_2O$ and $3.4x10^{-3}$ moles of $FeCl_3.6H_2O$, 2.5 ml 12.06 M HCl, and 7 ml PMAA to 50 ml with deoxygenated water in a two-necked round bottom flask. The molar ratio of Fe^{2+}/Fe^{3+} was 1:2. The precursor solution was always mixed under magnetic stirring during the addition of iron salts, acid and PMAA and nitrogen gas was passed through the vessel during the mixing. PMAA was added dropwise to the solution in order to obtain a good dispersion of polymer.

Subsequently, an aliquot of the precursor solution was added by a help of burette to 1.5 M NaOH solution prepared with deoxygenated water under ultrasonic irradiation. The experimental set-up which can be observed at Figure 2.4 was used and the experimental conditions which were summarized at Table 2.1 were applied. Nitrogen gas was passed through the reaction vessel during ultrasonication.

After ultrasonication, the black solution was centrifuged at 4000 rev/min for 5 minutes. After isolating the black solid, the supernatant was decanted. The black product was washed five times using deoxygenated water and centrifuged at 8000 rev/min for the first three washing cycles and then at 10000 rev/min for the last two washing cycles. The black product was finally washed with 0.01 M HCl and centrifuged at 13500 rev/min. The resulting PMAA-coated Fe_3O_4 nanoparticles were dispersed in deoxygenated water and final pH was adjusted to 3.5 with 0.01 M HCl. The samples were named as S4 and S5.

2.4 Characterization of Iron Oxide Nanoparticles

2.4.1 X-Ray Diffraction

Structural characterization of nanocomposites obtained is being evaluated by using Rigaku Miniflex X-ray diffractometer with Cu lamp operating at 35 kW and 15 mA in both Middle East Technical University (METU) Central Laboratory and METU Metalurgical and Materials Engineering Department. The raw data collected between 5° and 75^0 as 2θ was processed with Rigaku software and ICDD X-ray identification cards.

The crystal structures of the γ- Fe_2O_3 and Fe_3O_4 nanoparticles were determined using Hanawalt's method. This method relies on classifying powder patterns according to the three most intense lines in the X-ray pattern. The interplanar distances, d-values were determined from diffraction angles, of the three intense lines in the powder pattern (d1, d2, d3) along with their intensities (I) were used to search the X-ray identification cards.

The particle size of the powder samples was calculated by using Scherrer's formula. It is a technique based on measuring the full width of X-ray diffraction peaks at the half maximum height of the peak.

$$t = 0.94\,\lambda / B\cos\theta \qquad . [2.1]$$

In the Eq 2.1, t is the average particle size, λ is the wavelength of radiation of the X-ray beam used, B is the width of the peak at half of the maximum intensity (in radians) and θ is the half of the diffraction angle 2θ. For the particle size determination, magnetite (311) peak, which was the most intense peak, was used.

In order to calculate the lattice constant of the samples, the Bragg's Law was used,

$$n\,\lambda = 2\,d\,\sin\theta \qquad [2.2]$$

where n is an integer determined by the order given, λ is the wavelength of X-rays, d is the interplanar spacing between the planes in the atomic lattice, and θ is the angle between the incident ray and the scattering planes. Then, using the Eq. [2.3], the lattice constant, a, for the crystal structure was calculated.

$$a = d_{hkl}\sqrt{h^2 + k^2 + l^2} \qquad . [2.3]$$

2.4.2 Laser Particle Sizer

Malvern Mastersizer 2000 in METU Central Laboratory was used for the measurement of the agglomerate size of PMAA-coated Fe_3O_4 nanoparticles by using laser diffraction technique. Mie scattering is used as the measurement principle. The Mie scattering includes both diffraction and diffusion of the light around the particle in its medium. The light sources are helium neon laser for red light and solid state light source for blue light.

The particle size measurement provides volume weighted mean diameter (De Brouckere mean diameter, D[4,3]), the surface area weighted mean diameter (Sauter mean diameter, D[3,2]) and the specific surface area of the particles. The formula which is used to calculate different mean diameters was as follows:

$$D[m,n] = \left[\frac{\Sigma\, d_i^{m-3} V_i}{\Sigma\, d_i^{n-3} V_i}\right]^{1/(m-n)} \qquad [2.4]$$

The formula used to calculate the specific surface area is 6/D[3,2]. [2.5]

2.4.3 Zeta Potential Measurements

Malvern Nano ZS90 System was used for the zeta potential measurements of the PMAA-coated Fe_3O_4 nanoparticles in METU Central Laboratory.

2.4.4 Magnetic Measurements

Quantum Design Physical Property Measurement System was used at ±7 Tesla with VSM mode A vibrating sample magnetometer (VSM) is a device in which a sample is vibrated in a uniform magnetizing field and direct magnetization measurements of the sample is performed. The instrument allows precise magnetization measurements to be made as a function of temperature, magnetic field strength, and crystallographic orientation [91].

The magnetization data is determined with respect to room temperature and obtained M-H hysteresis curves give some important parameters about the remanent magnetism, coersive field and saturation magnetization values of the nanoparticles produced.

2.4.5 Scanning Electron Microscope

QUANTA 400F Field Emission Scanning Electron Microscope (FE-SEM) in METU Central Laboratory was used for the characterization and particle size identification of both uncoated and PMAA-coated Fe_3O_4 nanoparticles. The samples are diluted fifty times and 0.25 µl aliquots were placed on carbon tapes. The samples were left overnight for drying and then analyzed.

CHAPTER 3

RESULTS AND DISCUSSION

Throughout this study, two types of iron oxide nanoparticles, namely maghemite (γ-Fe_2O_3) and magnetite (Fe_3O_4) were prepared. The stabilization of iron oxide nanoparticles were achieved by dispersing maghemite in a sol-gel matrix and magnetite in a PMAA matrix.

3.1 Synthesis of Iron Oxide Nanoparticles in Sol-Gel Matrix

There are three main parameters that influence the maghemite phase formation during sol-gel process: The type of the precursors used, the calcination temperature and the surface to volume ratio of the sols.

3.1.1 The Type of Iron Salt

Sol-gel technique was used for the synthesis of maghemite (γ- Fe_2O_3) nanoparticles. Two different types of iron salt, $Fe(NO_3)_3.9H_2O$ and $FeCl_3.6H_2O$, were used as precursors and their influence on the formation of maghemite phase were examined. The same procedure described in Section 2.3.1 was applied for each type of iron salt, and the formed fresh monolithic gels were powdered and characterized by XRD. The XRD spectra of two different salts can be observed in Figure 3.1 and Figure 3.2.

From X-ray diffraction patterns, it was observed that while $Fe(NO_3)_3.9H_2O$ favoured the formation of gamma phase of iron oxide (Figure 3.1), $FeCl_3.6H_2O$ gave rise to hematite, alpha phase of iron oxide formation (Figure 3.2). These differences in the

resulting iron oxide phases could originate partially during the hydrolysis of the iron salts inside the silica pores. It is well-known that the composition and structure of iron (III) (hydrous) oxide formed in water depend on the preparation conditions such as Fe^{3+} concentration, the nature of the anion present and pH [92]. Hydrolysis of the iron salt proceeds by the formation of monomers and dimers of iron (III) ions, followed by the condensation of polymeric species. The polymers formed in the case of nitrates are presumed not to include the nitrate ion in the polymer chain, whereas the polymers formed in the chloride solution contain some chloride ions in place of the hydroxyl ions [93]. The next step in the precipitation process is the formation of oxybridges. In the presence of chloride ions, β-FeOOH is produced initially which later converts to α-Fe_2O_3 by heating [94]. From nitrate solutions, γ-FeOOH can be precipitated which directly transforms by heating to γ-Fe_2O_3 [95]. Therefore, γ-Fe_2O_3 nanocomposites should be preferentially formed through the reduction-oxidation of initially precipitated iron oxide-hydroxide polymeric material. However, it is clear that the nature of our nanocomposites formed in an organic medium (ethanol) depends on the type of the salt precursor [92].

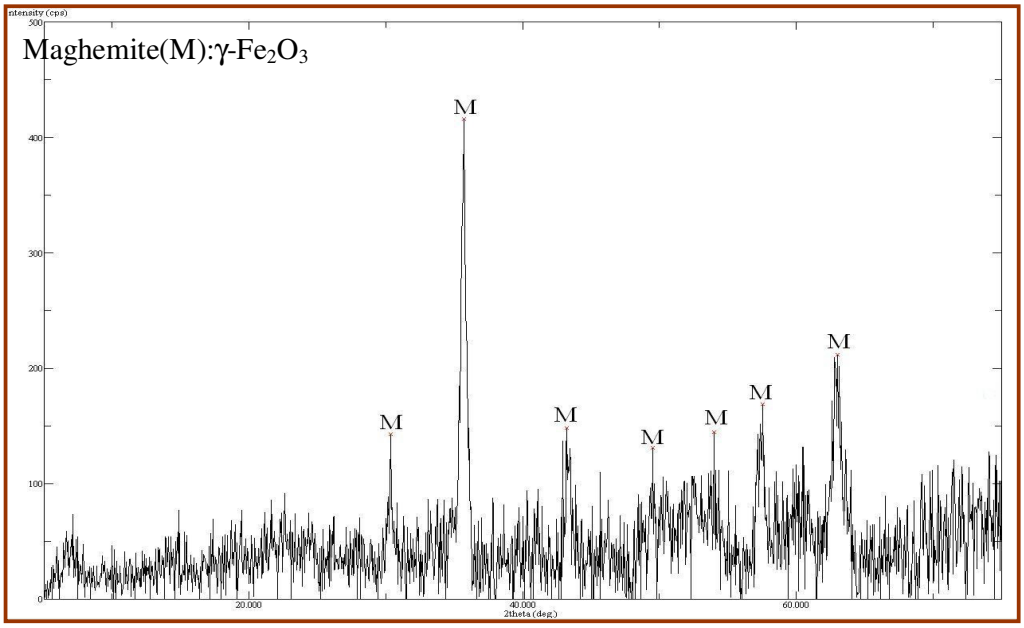

Figure 3.1 X-Ray diffraction pattern of Fe_2O_3-SiO_2 nanocomposite, salt used: $Fe(NO_3)_3.9H_2O$, S/V=0.04, heated at 400^oC

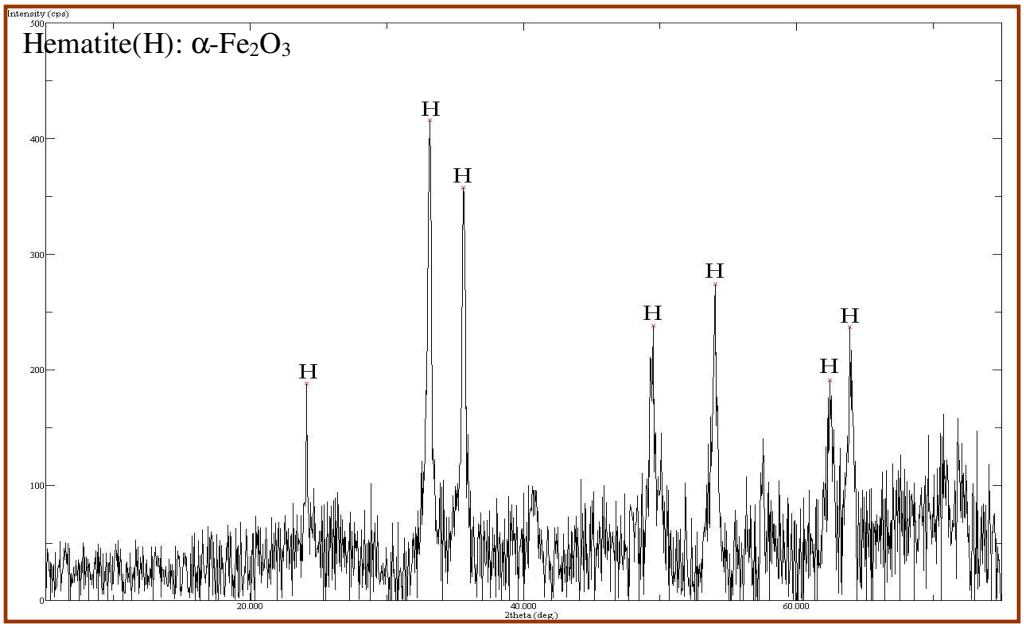

Figure 3.2 X-Ray diffraction pattern of Fe_2O_3-SiO_2 nanocomposite, salt used: $FeCl_3.6H_2O$, S/V=0.04, heated at 400^oC

3.1.2. The Calcination Temperature

Two different calcination procedures were applied to the iron oxide nanoparticles in order to observe the dominant phase of iron oxide. Some of samples were treated at a higher temperature in air, with increments of 50 °C from 150 °C up to 500°C, kept for 30 min at each stage and up to 900 °C with increments of 100°C, kept for one hour at each stage. Some of the samples were only heated to 400 °C for 4 h in air to observe the effect of heat treatment temperature on the phases produced in the Fe_2O_3-SiO_2 nanocomposite.

In the literature, the transition from γ to α phase has been reported to occur at 380°C for particles with an average size of 30 nm, and at 500°C for particles of 10 nm [96]. The diffractograms obtained by heat treating the gels at 900°C can be identified as consisting of α-Fe_2O_3 (hematite) antiferromagnetic crystalline phase (rhombohedral crystal system) (Figure 3.3). However, the peaks of the diffractograms obtained by heat treating the gels at 400°C can be identified mainly as γ-Fe_2O_3 (maghemite) ferrimagnetic crystalline phase (tetragonal crystal system) (Figure 3.4). There are some small peaks corresponding to α-Fe_2O_3 (hematite) on the same XRD spectrum. In the case of samples obtained from nitrate salts, temperatures higher than 400°C give rise to the transformation of maghemite into hematite due to a reaction with the matrix.

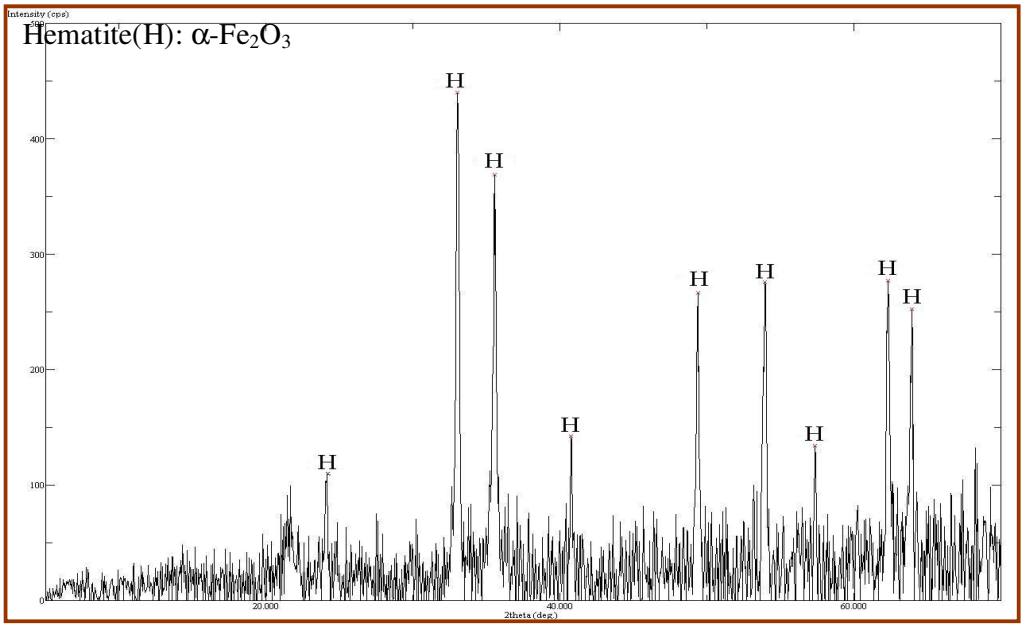

Figure 3.3 X-Ray diffraction pattern of Fe_2O_3-SiO_2 nanocomposite; salt used: $Fe(NO_3)_3.9H_2O$, S/V=0.03, heated at 900^oC

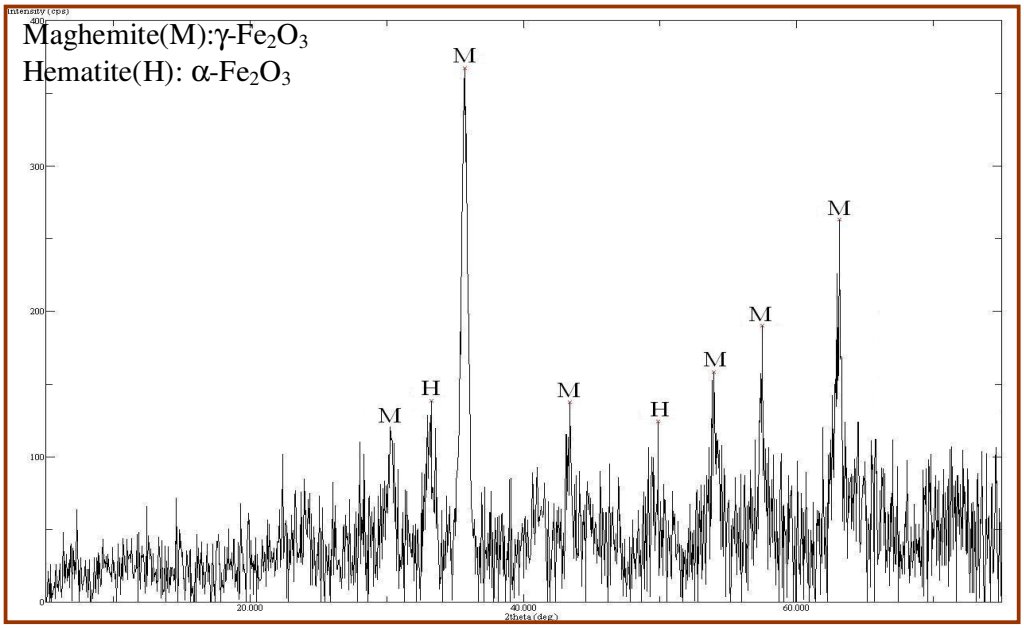

Figure 3.4: X-Ray diffraction pattern of Fe_2O_3-SiO_2 nanocomposite; salt used: $Fe(NO_3)_3.9H_2O$, S/V=0.03, heated at 400^oC

3.1.3 The Surface to Volume Ratio (S/V) of the Sols

S/V ratio was changed from 0.03 to 0.04 to investigate the maghemite formation. X-ray diffraction patterns given in Figures 3.5 and Figure 3.6 were obtained for two different S/V ratios, 0.03 and 0.04, respectively. For the samples gelated with lower S/V ratio, the X-ray patterns show well defined peaks. As the S/V ratio increases, it can be observed that the peak intensities start to decrease (Figure 3.6). From these results it can be concluded that the evaporation process during gelation plays an important role in the crystallization of the γ-Fe_2O_3 particles. The higher evaporation rate seems to be decisive for obtaining samples with smaller particle sizes [96]. By changing the S/V ratio, it is possible to control the gelation process in such a way that higher S/V ratio leads to smaller pore size of the matrix. The matrix structure is an important factor affecting the particle size of the nanocomposites [96].

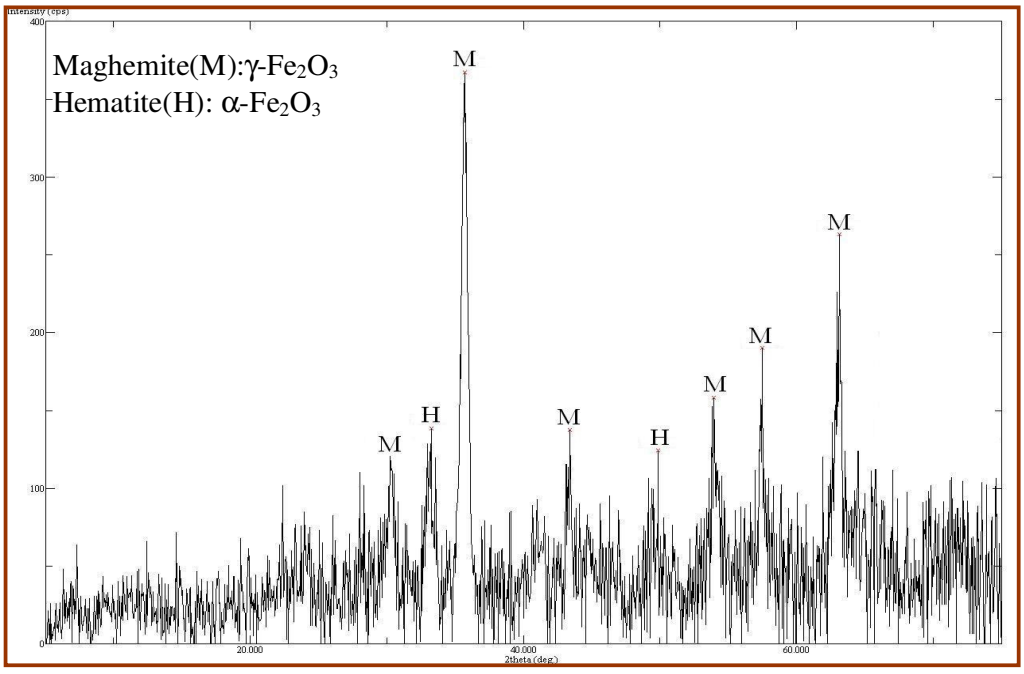

Figure 3.5 X-Ray diffraction patterns of Fe_2O_3-SiO_2 nanocomposites heated at 400^{o}C with S/V=0.03

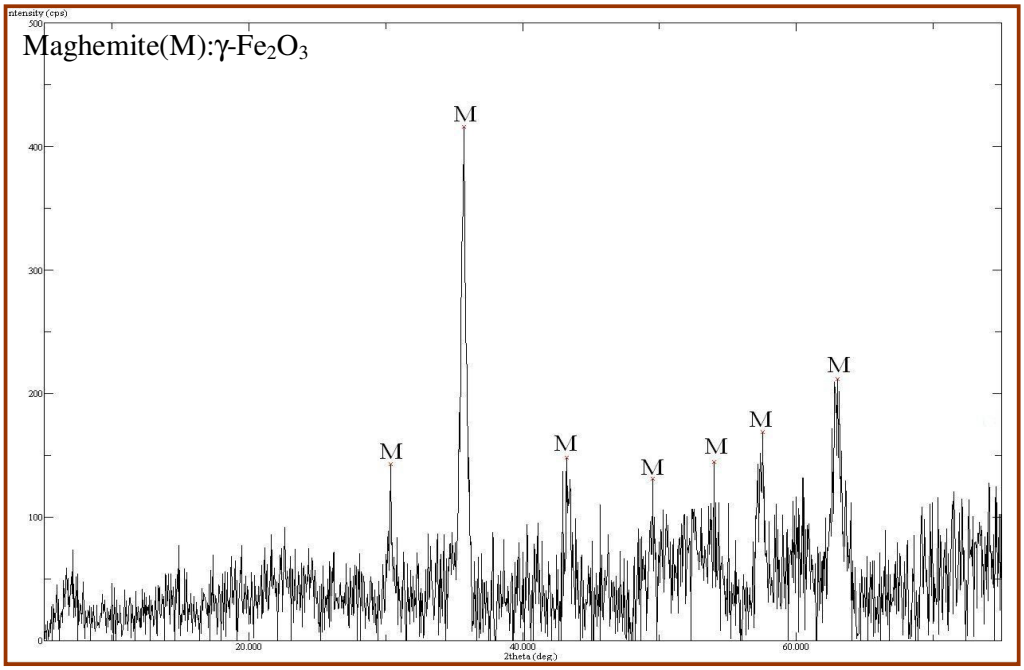

Figure 3.6 X-Ray diffraction patterns of Fe_2O_3-SiO_2 nanocomposites heated at 400°C with S/V=0.04

3.1.4 Magnetic Properties of Maghemite Nanoparticles in Sol-gel Matrix

The saturation magnetization values at 8 K increase up to a maximum of 8 emu/g obtained for the sample heat treated at 400ºC for S/V ratio equal to 0.04 (Figure 3.7). The saturation magnetization value is far from the reported value for bulk γ-Fe_2O_3 (74 emu/g), but these values are in fairly good agreement with the values measured in γ-Fe_2O_3 particles of similar size in sol-gel matrix [97, 98]. Surface and finite size effects have been also reported as being responsible for the decrease in the magnetic properties of nanoparticles [98].

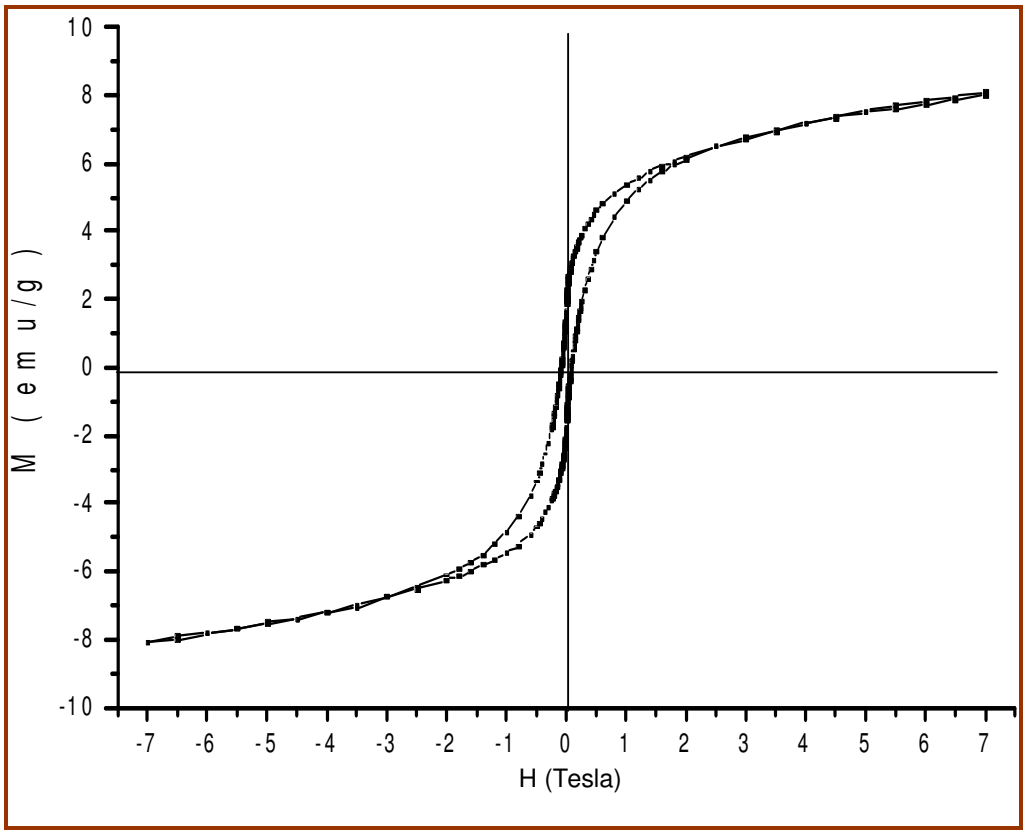

Figure 3.7 Hysteresis loop (M-H curves) of sample heat treated at 400^{o}C for the S/V ratio of 0.04. The curve was recorded at the temperature 8 K.

3.2 Synthesis of Poly(methacrylic acid)-Coated Magnetite (Fe_3O_4) Nanoparticles

Amorphous iron oxide nanoparticles have served as substrates for the self-assembly of poly(methacrylic acid) (PMAA). Preparation of PMAA coated magnetite particles was accomplished either *ex situ*, that is, the Fe_3O_4 nanoparticles were prepared first and then subjected to the PMAA solution under agitation or *in situ* where the iron oxide nanoparticles were synthesized in the presence of PMAA.

In situ preparation of magnetite nanoparticles was done previously in our laboratory via co-precipitation of iron salts under magnetic stirring in the presence of aqueous PMAA solution [99]. The influences of the process temperature, the PMAA content and the addition of surfactant on the PMAA-coated magnetite nanoparticles had been investigated and optimized [87]. Characterization studies have showed us that the formed particles are the aggregates of several small size (about 8 nm) Fe_3O_4 nanoparticles inside the micron sized PMAA matrix. The surface weighted mean sizes of PMAA-coated magnetic agglomerates were determined by using the laser diffraction technique and found to be range from 1.5 μm to 3 μm.

In this study, the effects of ultrasonic agitation on the surface weighted mean sizes of PMAA-coated magnetic agglomerates were investigated. The same optimized conditions [87] were used for the preparation of PMAA-coated magnetic agglomerates in the presence of ultrasonic agitation. The goal of this study is to decrease the size of the agglomerates and increase the specific surface area.

These prepared magnetic nanoparticles are planned to be used in biologic separation process. As it is well known, the chemical reactivity and the reaction rates of the particles increase as the specific surface area increases, which is inversely proportional with the particle size [11] since the atoms situated at the surface of a particle have less neighbours than bulk atoms. Because of this lower coordination, surface atoms are less stabilized than bulk atoms and have higher average binding energy per atom which leads to easy bonding with the contacting materials [22]

3.2.1 *Ex Situ* Synthesis of PMAA-coated Magnetite Nanoparticles, Two-step Procedure

As stated previously in Section 2.3.2.1, this is a two step process. After Fe_3O_4 nanoparticles were prepared under ultrasonic irradiation, the polymer coating of the nanoparticles was realized using either magnetic stirrer or ultrasonic probe. The effect of these two types of agitations on particle size distribution was discussed on the following sections.

3.2.1.1 Synthesis of Magnetite Nanoparticles under Ultrasonic Agitation

The Fe_3O_4 nanoparticles were synthesized by co-precipitating the iron precursors (ferrous sulfate heptahydrate ($FeSO_4.7H_2O$) and ferric trichloride hexahydrate ($FeCl_3.6H_2O$) in the acidic solution) in 1.5 M NaOH. Ultrasonic irradiation was used during the co-precipitation of iron salts instead of magnetic stirring. The ultrasonication conditions were summarized in Table 2.1.

The estimated reaction taking place is as follows:

$$FeSO_4.\ 7\ H_2O\ (aq.) + 2\ FeCl_3.\ 6\ H_2O\ (aq.) + 8\ NaOH\ (aq.) \rightleftharpoons Fe_3O_4\ (s) + 23\ H_2O\ (l) + Na_2SO_4\ (aq.) + 6\ NaCl\ (aq.) \quad [100]$$

The black solid product was separated from solution by aid of centrifugation and washed several times with de-oxygenated water and HCl. At last, the black solid dispersed in de-oxygenated water at pH 3. The uncoated Fe_3O_4 nanoparticle sample was named as S1.

The XRD pattern of the S1 was illustrated in Figure 3.8. All detected diffraction peaks could be attributed to the characteristic peaks of spinel iron oxide (γ-Fe_2O_3 or Fe_3O_4) according to ICDD X-ray identification cards, indicating that sample did not contain crystalline hematite (α-Fe_2O_3) or iron hydroxides.

In the X-ray diffraction pattern, the peak at 40.5° indicated with a question mark could not be identified. It could not be attributed to either the magnetite phase or the other iron oxide phases such as maghemite or hematite.

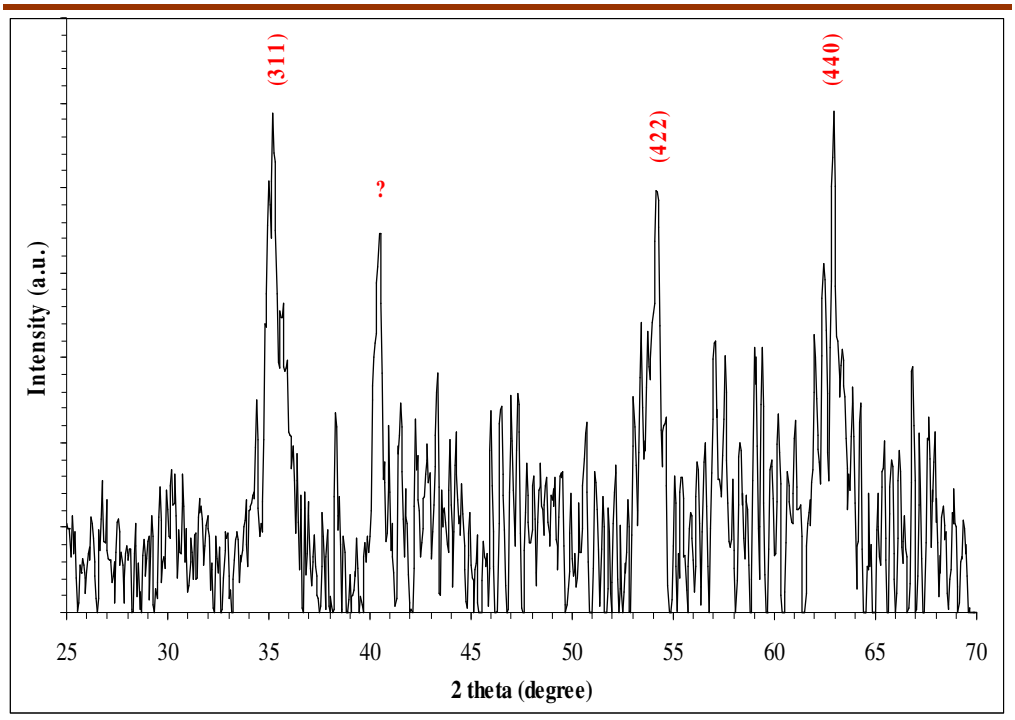

Figure 3.8 The X-ray diffraction pattern of S1, Fe_3O_4 nanoparticles synthesized under ultrasonic agitation

The lattice constant, a, of the sample was calculated as 0.840 nm from the most intense peaks according to Bragg's Law, Eq. [2.3] and Eq. [2.4]. The lattice constants of maghemite (γ-Fe_2O_3) and magnetite (Fe_3O_4) are reported as 0.835 nm and 0.839 nm, respectively. The main crystalline phase of synthesized sample could be identified as magnetite since the calculated and theoretical lattice constants, a and the interplanar distances, d matched. The results are summarized in Table 3.1.

Table 3.1 Theoretical and measured characteristics of S1, Fe_3O_4 nanoparticles synthesized under ultrasonic agitation, by XRD

(h k l)	Measured 2θ (°)	Theoretical d_{hkl} *	Calculated d_{hkl}	Calculated a (nm)
(3 1 1)	35.2	2.531	2.549	0.840
(4 4 0)	62.95	1.484	1.477	0.835
(4 2 2)	54.15	1.713	1.693	0.830

*ICDD Card No: 75-1610

In addition, the average size of the iron oxide nanoparticles was calculated as 9.8 nm using the Scherrer equation, Eq. [2.1]. It is well known that Scherrer equation provides a volume-weighted average of the grain size and underestimates the grain size by 11-38% [101]. In addition, 2θ values of characteristic peaks of both maghemite and magnetite are very similar in XRD spectrum. Probably, the presence of two iron oxide phases; magnetite and maghemite caused the broadening of the characteristic peaks in the spectrum. Then, the half peak-width of the characteristic peaks got wider which resulted in the underestimation of the calculated particle size.

The field emission scanning electron microscope (FE-SEM) images and energy-dispersive X-ray spectrum (EDX) for S1, Fe_3O_4 nanoparticles synthesized under ultrasonic agitation, were given in Figure 3.9 and Figure 3.10, respectively. Well-dispersed magnetite nanoparticles could be clearly observed on the FE-SEM image.

EDX spectrum showed the elemental analysis. The presence of iron and oxygen could be clearly observed. The sample was coated with gold for better resolution before taking the image. The Au peaks could be attributed to that coating. The reason of high intensity carbon peak was the carbon tape on which the sample was prepared.

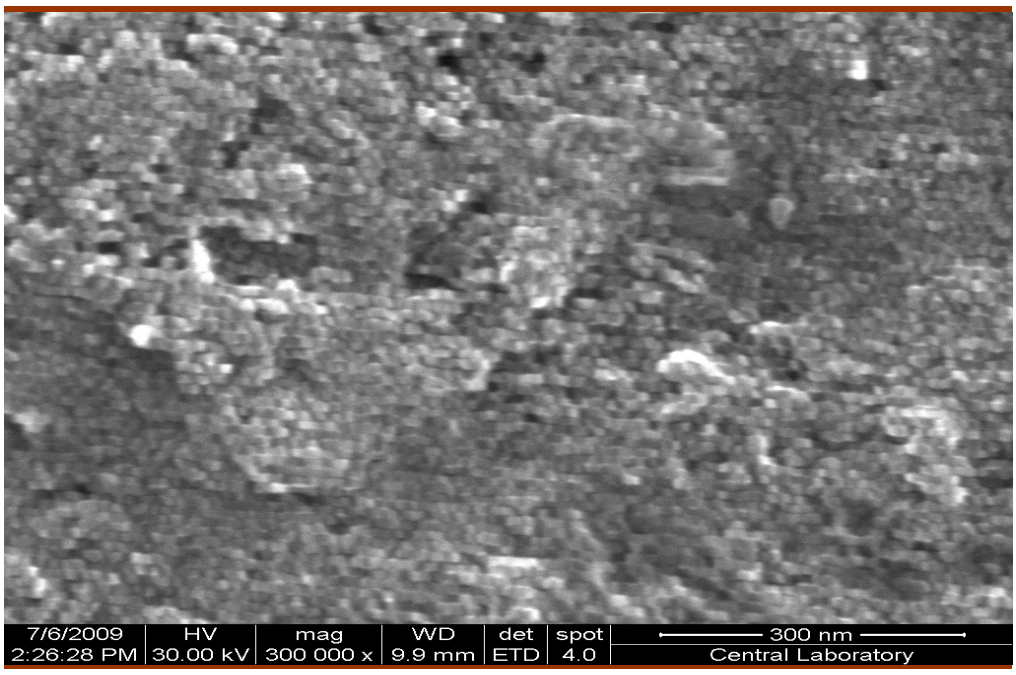

Figure 3.9 FE-SEM image of S1, Fe_3O_4 nanoparticles synthesized under ultrasonic agitation, at 300000x magnification coated with Au

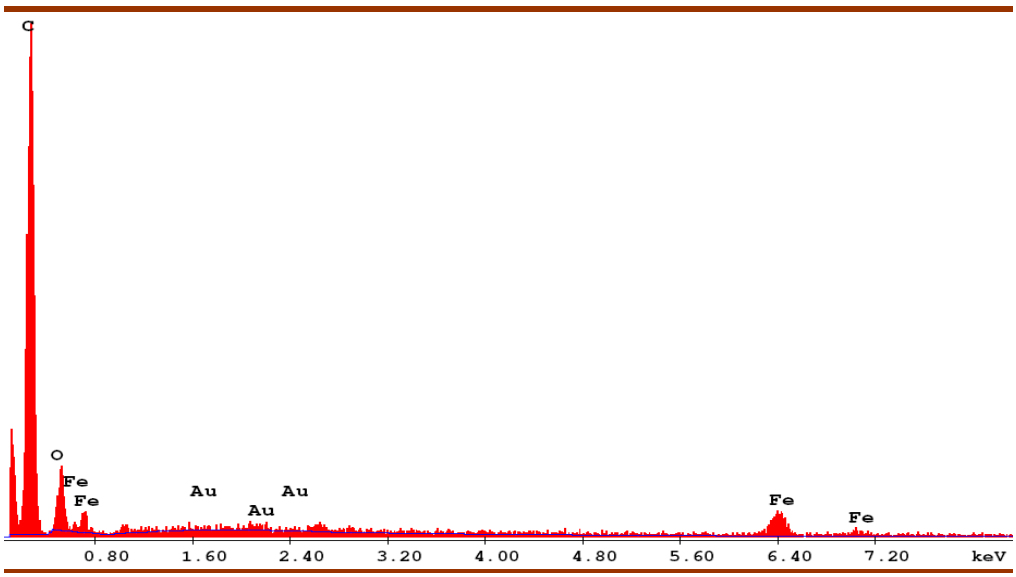

Figure 3.10 EDX spectrum of Fe_3O_4 nanoparticles synthesized under ultrasonic agitation

In the Figure 3.11, the particle size distribution graph of S1, Fe_3O_4 nanoparticles synthesized under ultrasonic agitation, could be observed. According to the calculations done by using the Eq 2.4 and 2.5, D[4,3], D[3,2] and the specific surface area were measured as 123 nm, 102 nm and 59.1 m^2/cm^3, respectively. The particle size of magnetite nanoparticles calculated using the X-ray spectrum was 9.8 nm. It could be clearly observed that the particle size calculated by using Scherrer equation from X-ray spectrum and the particle size obtained from laser particle sizer differed. The possible reason of this difference was that the approximately 12 magnetite nanoparticles were aggregated due to interaction of the surfaces when the sample was dispersed in water during the laser particle size measurement.

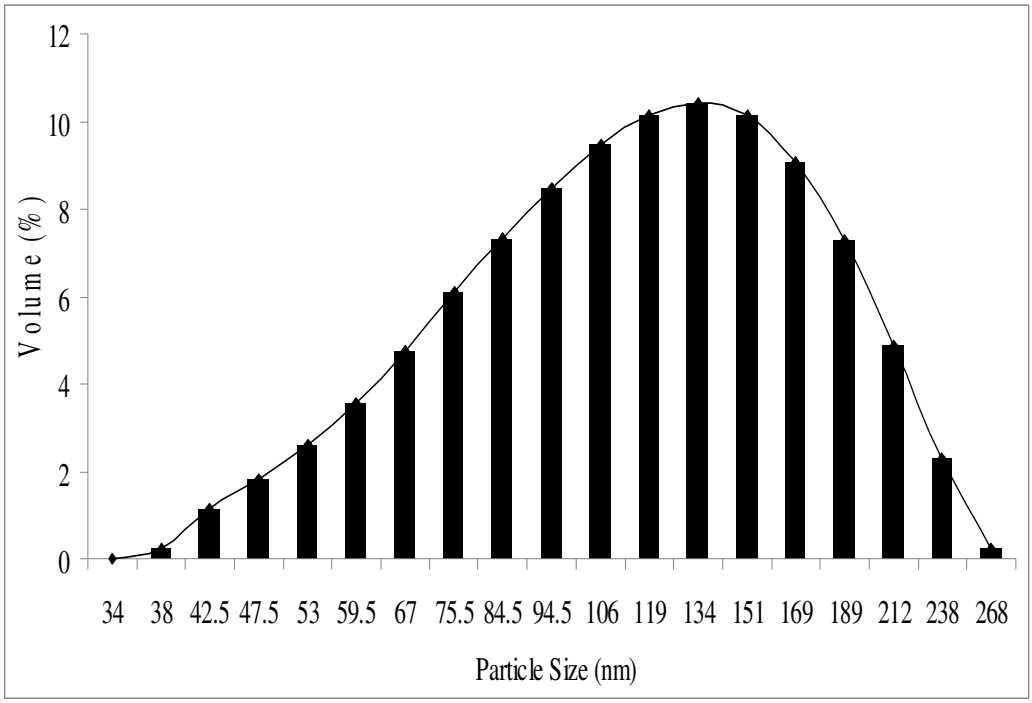

Figure 3.11 Particle size distribution of S1, Fe_3O_4 nanoparticles synthesized under ultrasonic agitation, obtained from laser particle sizer

3.2.1.2 *Ex Situ* Synthesis of PMAA Coated Magnetite Nanoparticles under Magnetic Stirring

The polymer coating of the nanoparticles was realized under magnetic stirring after the synthesis of the Fe_3O_4 nanoparticles under ultrasonic agitation. These *ex situ* prepared PMAA coated magnetic nanoparticle agglomerates were named as S2.

The particle size distribution graph for S2, *ex situ* prepared PMAA coated magnetic particles under magnetic stirring, is given in Figure 3.12. D[4,3], D[3,2] and the specific surface area were calculated as 134.9 μm, 122.6 μm and 0.049 m^2/cm^3, respectively.

It was necessary to make a distinction between the concept of the particle size of Fe_3O_4 nanoparticles and the particle size of PMAA coated Fe_3O_4 nanoparticles. From this point to forward, while commenting on particle size, uncoated Fe_3O_4 nanoparticle would be called as primary particle since it constituted the basis. The particle size of PMAA coated magnetite nanoparticles would be referred as agglomerate size.

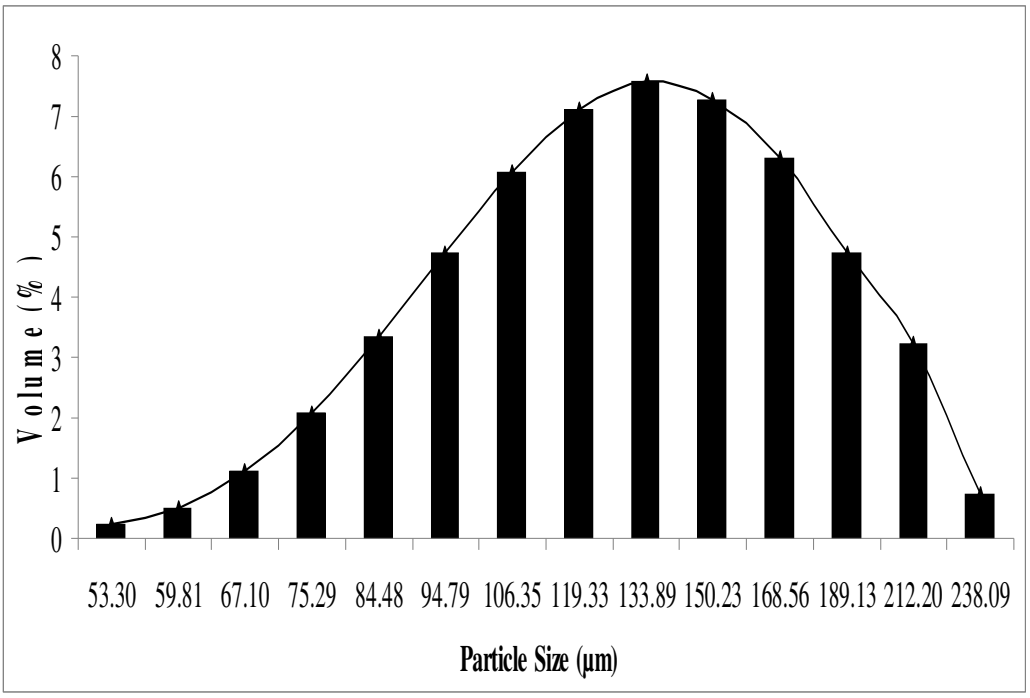

Figure 3.12 Agglomerate size distribution of S2, e*x situ* prepared PMAA coated magnetite particles under magnetic stirring, obtained from laser particle sizer

3.2.1.3 *Ex Situ* Synthesis of PMAA Coated Magnetite Nanoparticles under Ultrasonic Agitation

The iron oxide particles synthesized were coated with PMAA under the influence of ultrasonic agitation. These *ex situ* prepared PMAA coated magnetic particles were named as S3. The agglomerate size distribution graph for S3 is given in Figure 3.13.

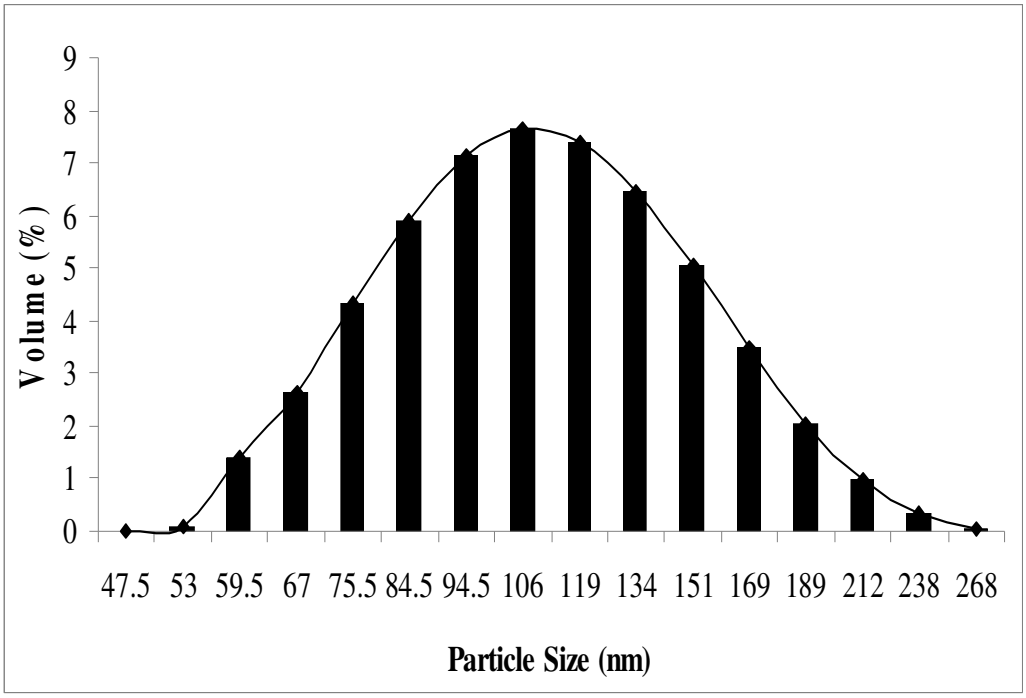

Figure 3.13 Agglomerate size distribution of S3, *ex situ* prepared PMAA coated magnetite nanoparticles under ultrasonic agitation, obtained from laser particle sizer

According to agglomerate size measurements, D[4,3], D[3,2] and the specific surface area were measured as 115.6 nm, 105.4 nm and 56.9 m^2/cm^3, respectively.

The agglomerate size results obtained by laser particle sizer and summarized in Table 3.2 showed that the *ex situ* PMAA encapsulation of magnetite particles under magnetic stirring resulted in approximately 1000 fold larger particles in size when compared to magnetite particles encapsulated under ultrasonic agitation. It could be concluded that polymer coating carried out under ultrasonic agitation created drastic changes in particle size. Consequently, applying ultrasound for the *ex situ* encapsulation of magnetite nanoparticles with PMAA gave rise to smaller agglomerates and high specific surface area.

Table 3.2 The agglomerate sizes and specific surface areas of S2 and S3 obtained from laser particle sizer

Sample Name	D[4,3] Volume Weighted Mean Diameter	D[3,2] The Surface Area Weighted Mean Diameter	Specific Surface Area
S2, *Ex Situ* Synthesized PMAA Coated Magnetite Nanoparticles under Magnetic Stirring	134.9 x 10^3 nm	122.6 x 10^3 nm	0.049 m^2/cm^3
S3, *Ex Situ* Synthesized PMAA Coated Magnetite Nanoparticles under Ultrasonic Agitation	115.6 nm	105.4 nm	56.9 m^2/cm^3

3.2.2 *In Situ* Synthesis of PMAA Coated Magnetite Nanoparticles, One-Step Procedure

In one-step method, the synthesis of magnetite nanoparticles and encapsulation of them in PMAA were done by aid of ultrasonication in one step. The aqueous precursor solution was prepared by diluting a mixture of iron salts, HCl, and PMAA to 50 ml with deoxygenated water. The precursor solution was always mixed under magnetic stirring during the addition of iron salts, acid and PMAA. PMAA was added dropwise to the solution in order to obtain a good dispersion of polymer. Subsequently, an aliquot of the precursor solution was added to 1.5 M NaOH solution under ultrasonic irradiation. The polymer coated black product was washed and dispersed at pH 4.5. The ultrasonication period was 40 minutes. These *in situ* synthesized PMAA coated magnetic nanoparticle agglomerates were named as S4.

In XRD pattern of S4 is depicted in Figure 3.14. All detected diffraction peaks could be attributed to the characteristic peaks of spinel iron oxide (γ-Fe_2O_3 or Fe_3O_4) according to ICDD X-ray identification cards, indicating that sample did not contain crystalline hematite (α-Fe_2O_3) or iron hydroxides.

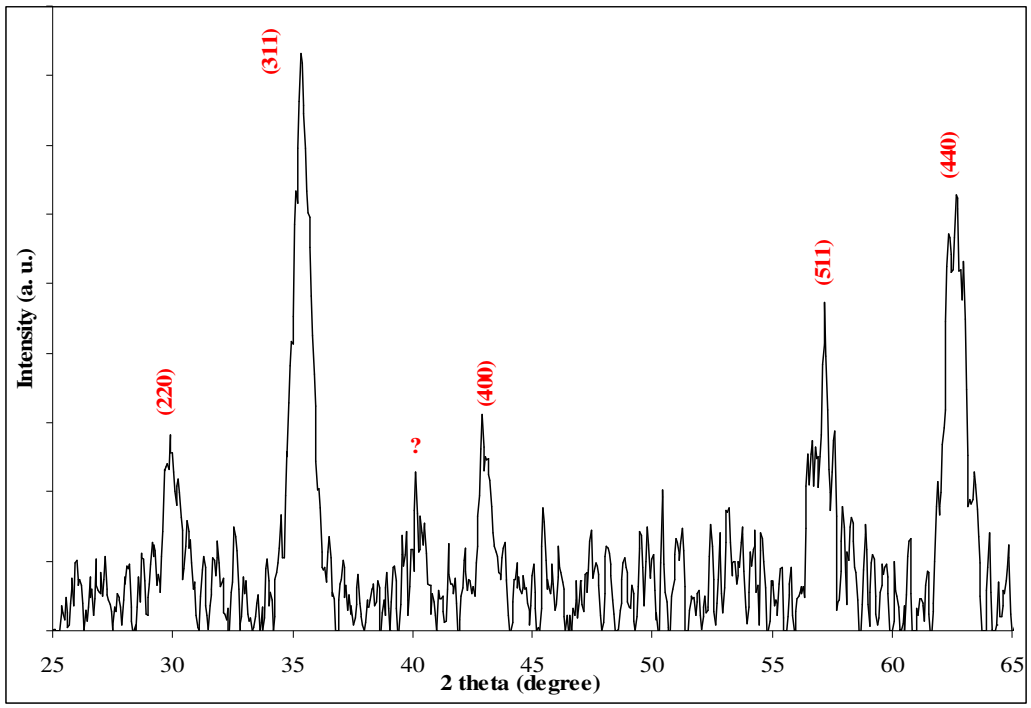

Figure 3.14 X-Ray diffraction pattern of S4, *in situ* prepared PMAA coated magnetite agglomerates under ultrasonic agitation

The average size of the primary magnetite nanoparticles inside the agglomerates was calculated as 9.7 nm using Eq. [2.1]. The lattice constant, a and the interplanar distances, d of the sample were calculated according to Eq. [2.3] and Eq. [2.4] and summarized in Table 3.3, indicating that the sample was mainly magnetite.

Table 3.3 Theoretical and measured characteristics of S4, *in situ* prepared PMAA coated magnetite agglomerates, by XRD

(h k l)	Measured 2θ (°)	Theoretical d_{hkl} *	Calculated d_{hkl}	Calculated a (nm)
(3 1 1)	35.35	2.531	2.539	0.842
(4 4 0)	62.65	1.484	1.483	0.839
(5 1 1)	57.2	1.615	1.610	0.837
(2 2 0)	29.9	2.968	2.988	0.845
(4 0 0)	42.9	2.099	2.108	0.843

* ICDD Card No: 75-1610

In the X-ray diffraction pattern shown in Figure 3.14, the peak at 40.15° indicated with a question mark could not be identified. It could not be attributed to either the magnetite phase or the other iron oxide phases such as maghemite or hematite. In order to investigate the basis of this peak, *in situ* synthesized PMAA coated magnetite agglomerates were subjected to heat treatment at 400°C for 4 hours and XRD spectrum was taken and depicted in Figure 3.15. The little shift in 2θ values and the broadening of the characteristic peaks indicated that the phase transformation from magnetite phase of iron oxide to maghemite occurred. Also, such an apparent decrease in the intensity of the peak at 40.15° was observed that it is not possible to distinguish the peak at 40.15° from the noise signals.

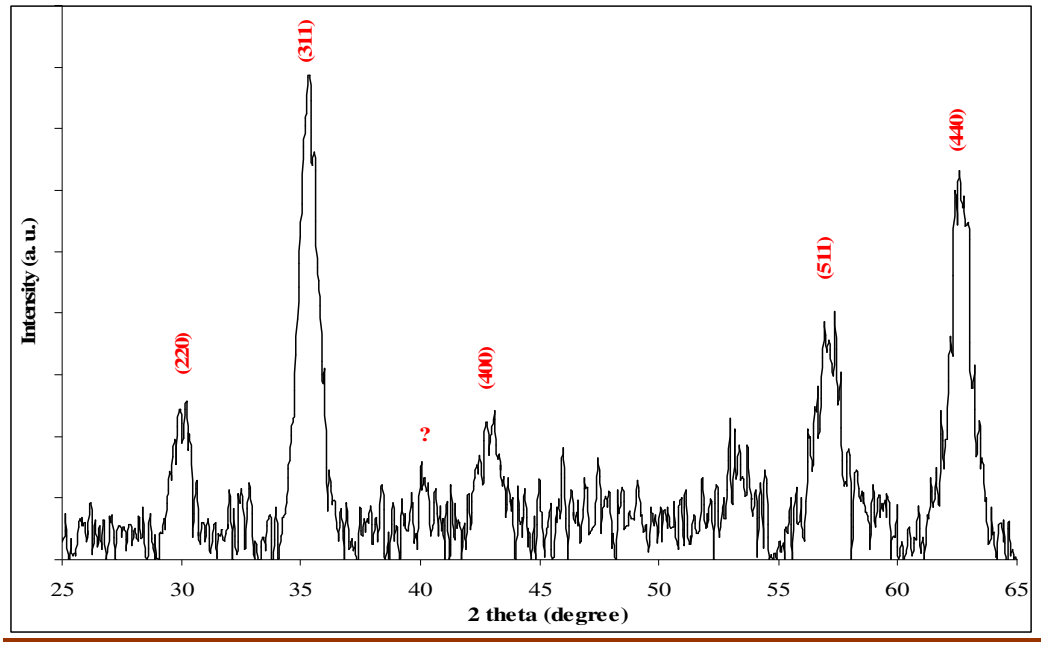

Figure 3.15 X-ray diffraction pattern of heat treated S4 at 400°C for 4 hours

Table 3.4 Theoretical and measured characteristics of heat treated S4 at 400°C for 4 hours, by XRD

(h k l)	Iron Oxide Phase	Measured 2θ (°)	Theoretical d_{hkl} *	Calculated d_{hkl}	Calculated a (nm)
(3 1 1)	Magnetite	35.35	2.531	2.539	0.842
	Maghemite	35.55	2.518	2.525	0.837
(4 4 0)	Magnetite	62.60	1.484	1.484	0.839
	Maghemite	62.95	1.476	1.476	0.835
(5 1 1)	Magnetite	56.95	1.615	1.617	0.840
	Maghemite	57.4	1.607	1.605	0.834
(2 2 0)	Magnetite	29.95	2.968	2.983	0.843
	Maghemite	30.2	2.953	2.959	0.837

* ICDD Card No: 75-1610 and 39-1346

The lattice constant, a and the interplanar distances, d of the sample, calculated according to Eq. [2.3] and Eq. [2.4] and summarized in Table 3.4 for both iron oxide phases, magnetite and maghemite indicated that the heat treated sample at 400°C had both phases together.

The agglomerate size distribution of S4, *in situ* prepared PMAA coated magnetite agglomerates under ultrasonic agitation, was measured utilizing laser particle sizer. The particle size distribution graph can be seen in the Figure 3.16.

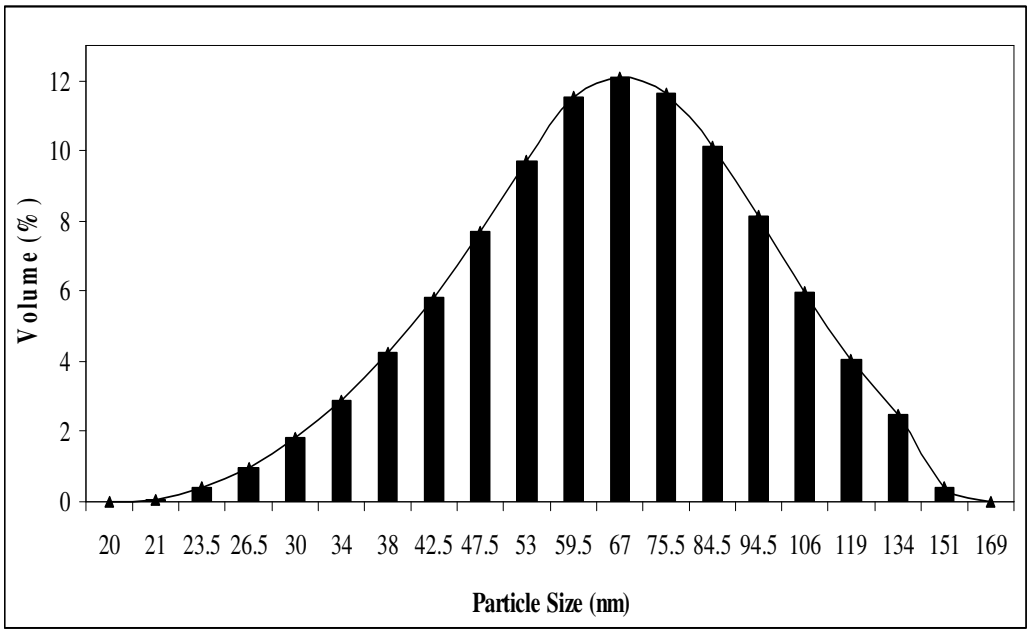

Figure 3.16 Agglomerate size distribution of S4, *in situ* prepared PMAA coated magnetite agglomerates under ultrasonic agitation, obtained from laser particle sizer

According to the calculations done by using the Eq. [2.4] and Eq. [2.5], D[4,3], D[3,2] and the specific surface area were measured as 69.9 nm, 61 nm and 98.4 m^2/cm^3, respectively.

The agglomerate size results obtained by laser particle sizer and summarized in Table 3.5 showed that the *in situ* prepared PMAA coated magnetite agglomerates under ultrasonic agitation in one-step, S4 were ½ fold smaller than the magnetite agglomerates which were *ex situ* encapsulated with PMAA in two-step process. Also, a 2 fold increase was observed in the specific surface area of PMAA coated magnetite agglomerates. Consequently, the *in situ* encapsulation of magnetite nanoparticles with PMAA by applying ultrasound in one step process gave rise to much smaller agglomerate size and higher specific surface area.

Table 3.5 The agglomerate sizes and specific surface areas of S2, S3 and S4 obtained from laser particle sizer

Sample Name	D[4,3] Volume Weighted Mean Diameter	D[3,2] The Surface Area Weighted Mean Diameter	Specific Surface Area
S2, *Ex Situ* Synthesized PMAA Coated Magnetite Nanoparticles under Magnetic Stirring	134.9 x 10^3 nm	122.6 x 10^3 nm	0.049 m^2/cm^3
S3, *Ex Situ* Synthesized PMAA Coated Magnetite Nanoparticles under Ultrasonic Agitation	115.6 nm	105.4 nm	56.9 m^2/cm^3
S4, *In Situ* Synthesized PMAA Coated Magnetite Nanoparticles under Ultrasonic Agitation	69.9 nm	61 nm	98.4 m^2/cm^3

FE-SEM images of *in situ* synthesized PMAA coated magnetic agglomerates under ultrasonic agitation, S4 are given in Figure 3.17:

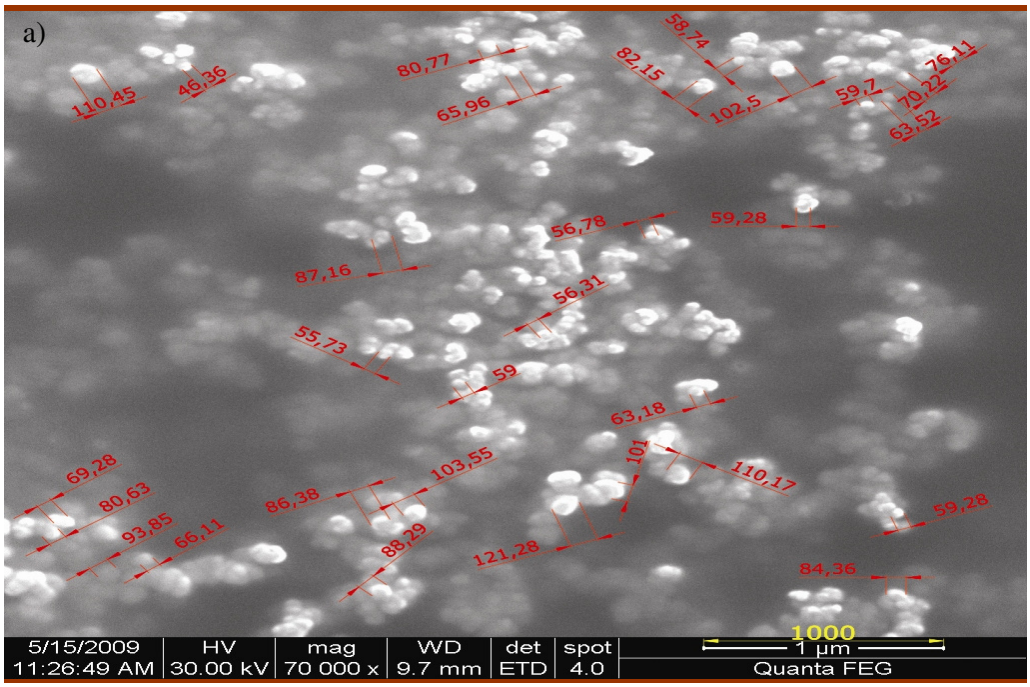

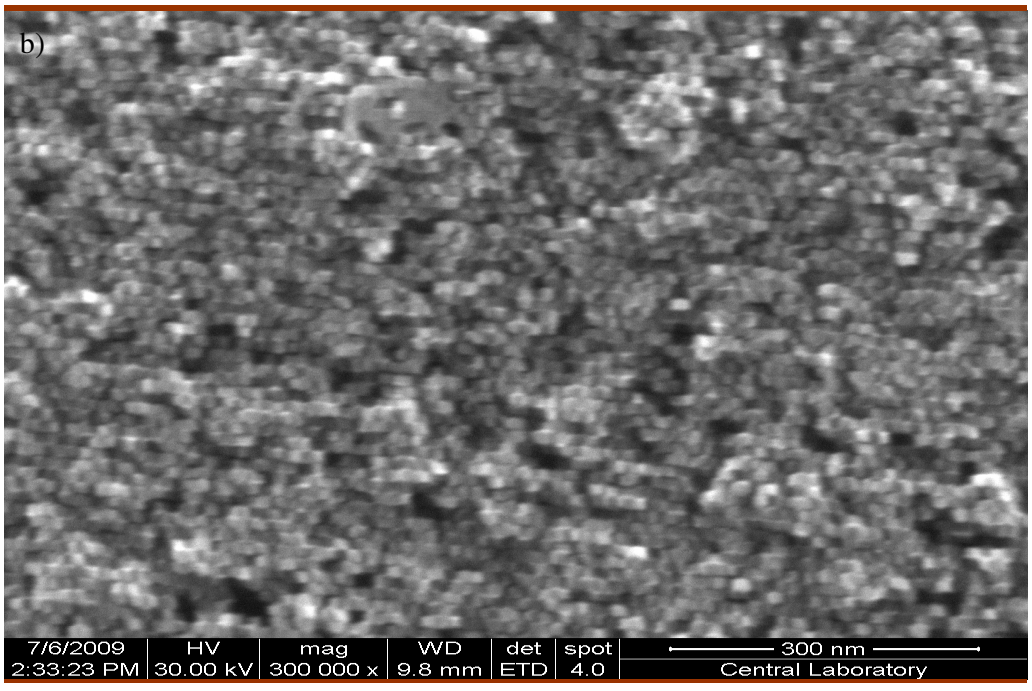

Figure 3.17 FE-SEM images of S4, *in situ* synthesized PMAA coated magnetite agglomerates under ultrasonic agitation a) at 70000x magnification b) at 300000x magnification coated with Au

A second agglomerate size distribution graph was prepared for sample S4 by processing FE-SEM image (Figure 3.17) with *AutoCAD* software program. The sizes of several individual agglomerates were measured by software and bar graph was prepared. This graph can be observed in Figure 3.18.

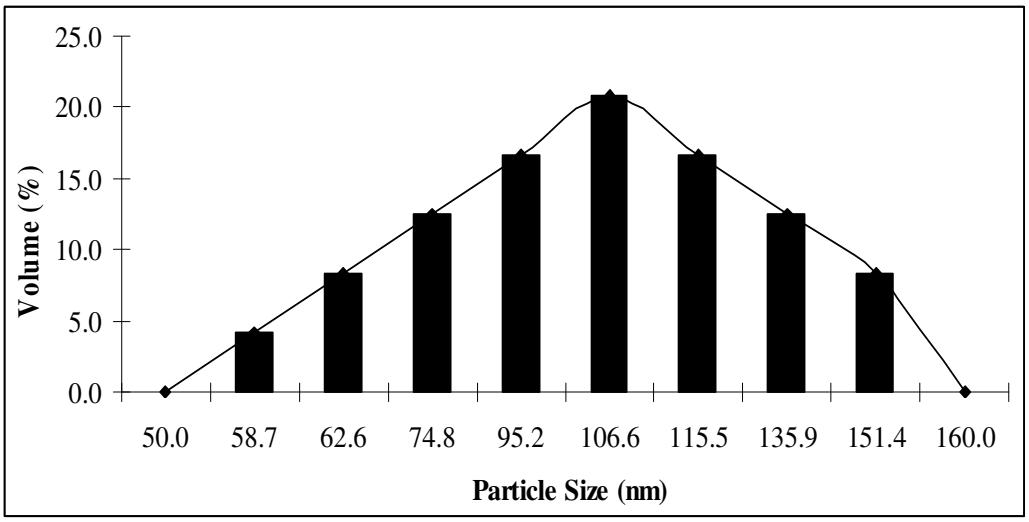

Figure 3.18 Particle size distribution of S4 prepared by using the size measurements obtained from FE-SEM image through *AutoCAD* software program

D[4,3], D[3,2] and the specific surface area for S4 were calculated as 103.9 nm, 96.8 nm and 62 m^2/cm^3, respectively .

There is quite a large difference between these two agglomerate size distribution calculations. The reason of the difference between the calculated values of two separate methods is the number of particles taken into consideration during evaluation process. The laser particle sizer measurement represents the whole sample but on the FE-SEM image, only a very small portion of the sample can be observed. Besides only well defined agglomerates with good resolution can be measured by *AutoCAD* software program.

The difference between the particle size of primary magnetite particle obtained from XRD (9.7 nm) and the particle size of PMAA-coated magnetite particles (61 nm) shows that more about 12 magnetite nanoparticles were aggregated and encapsulated in PMAA matrix.

3.2.2.1 The Effect of the Duration of Ultrasonic Agitation on particle size

During *in situ* sample preparation of the PMAA coated particles (S4), for 40 minutes ultrasonic agitation was applied. In order to investigate the effect of reaction period on the particle and agglomerate size, 20 minutes ultrasound irradiation was applied for the preparation of the samples (S5). All other parameters were kept the same. Thus, prepared sample was characterized as before using XRD, particle sizer, and FE-SEM. The XRD pattern for S5 is given in Figure 3.19.

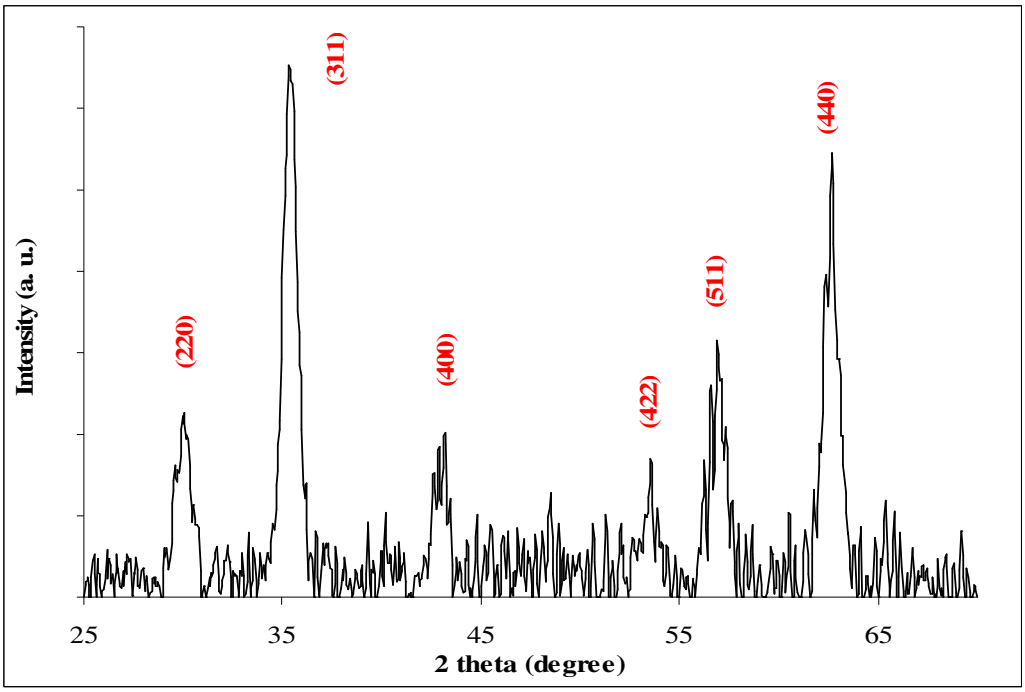

Figure 3.19 X-Ray diffraction pattern of S5, i*n situ* prepared PMAA coated magnetite agglomerates under 20 minutes ultrasonic agitation

The average size of the primary magnetite nanoparticles was calculated as 9.9 nm using Eq. [2.1]. The lattice constant, a and the interplanar distances, d of the sample were calculated according to Eq. [2.3] and Eq. [2.4] and summarized in Table 3.6, indicating that the sample is magnetite.

Table 3.6 Theoretical and measured characteristics of S5, *in situ* prepared PMAA coated magnetite agglomerates under 20 minutes ultrasonic agitation. by XRD

(h k l)	Measured 2θ (°)	Theoretical d_{hkl} *	Calculated d_{hkl}	Calculated a (nm)
(3 1 1)	35.3	2.531	2.542	0.843
(4 4 0)	62.7	1.484	1.482	0.838
(5 1 1)	56.9	1.615	1.618	0.841
(2 2 0)	29.95	2.968	2.983	0.844
(4 0 0)	43.15	2.099	2.097	0.839
(4 2 2)	53.55	1.713	1.712	0.838

* ICDD Card No: 75-1610

The FE-SEM image and EDX spectrum of sample S5 are given in Figure 3.20 identifies that PMAA-coated magnetite agglomerates were synthesized when 20 minutes ultrasonication was applied during the experiment.

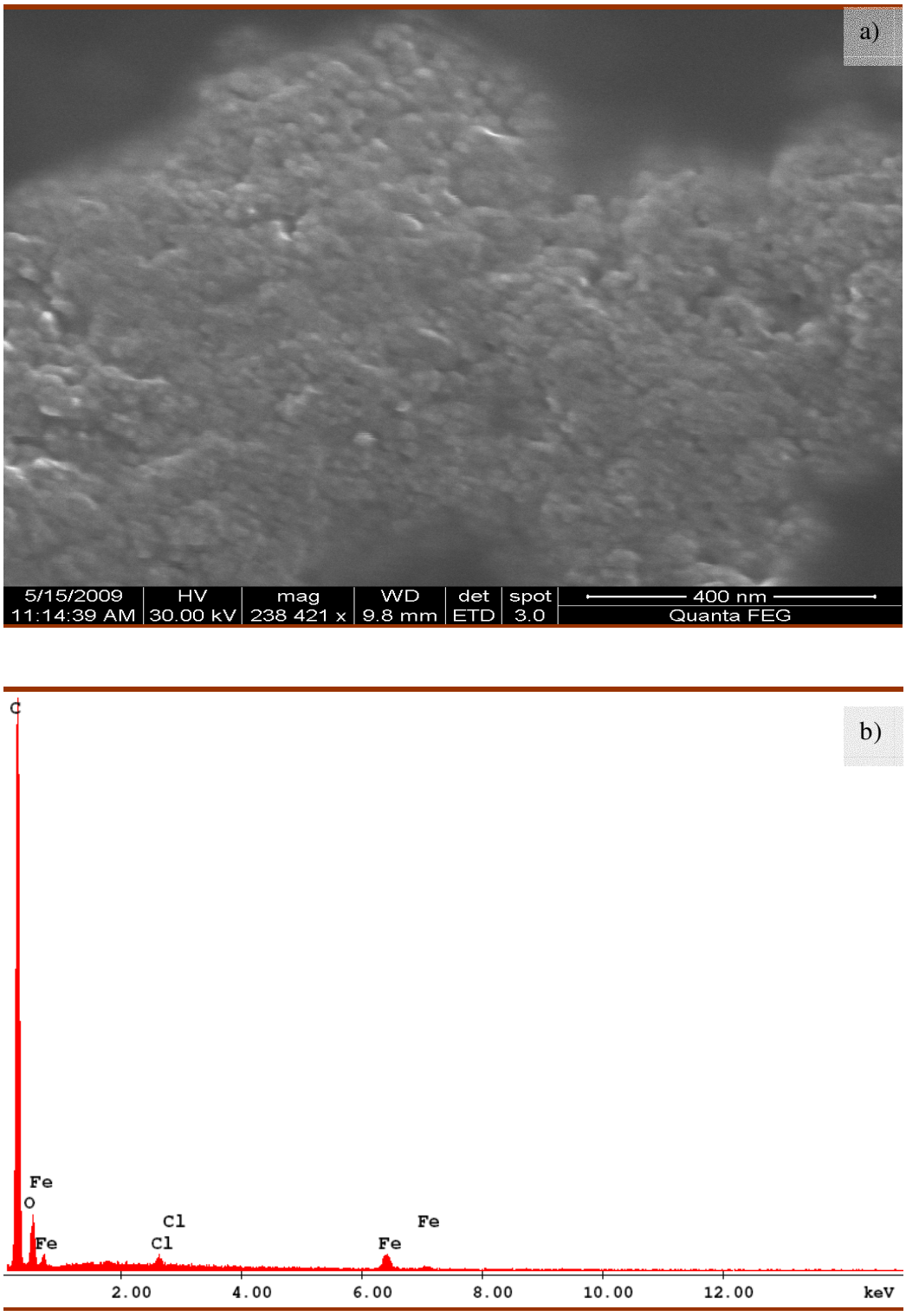

Figure 3.20 a) FE-SEM image and b) EDX spectrum of S5, *in situ* prepared PMAA coated magnetite agglomerates under 20 minutes ultrasonic agitation

When the agglomerate size was measured with laser particle sizer, D[4,3], D[3,2] and the specific surface area were found to be 156.9 nm, 141.9 nm and 42.3 m^2/cm^3, respectively (Figure 3.21).

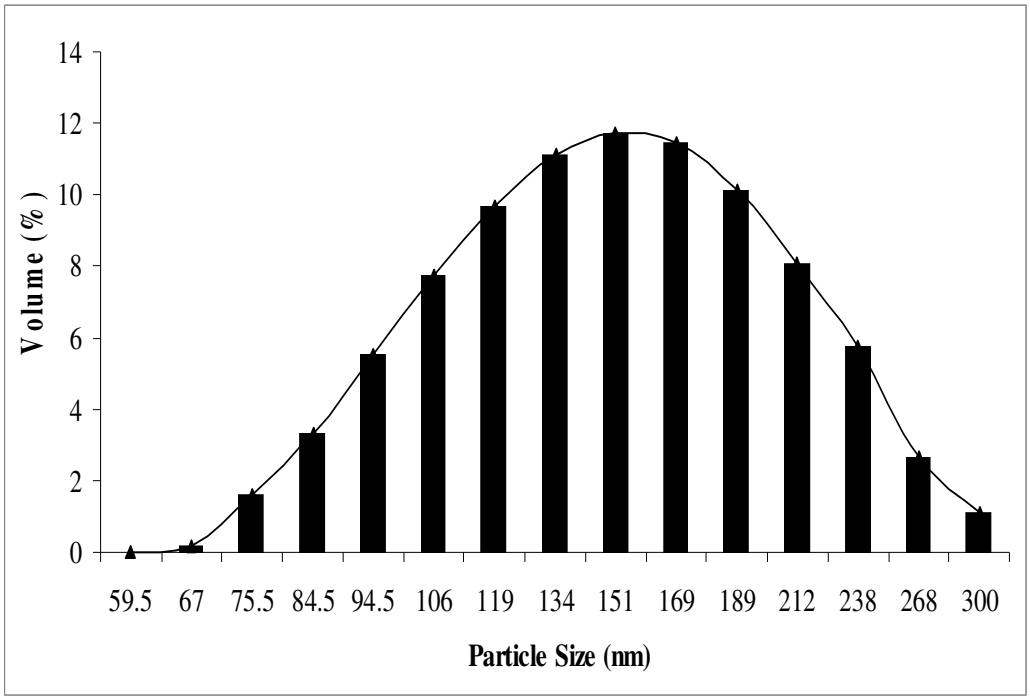

Figure 3.21 Particle size distribution of S5, *in situ* prepared PMAA coated magnetite agglomerates under 20 minutes ultrasonic agitation, obtained from laser particle sizer

The results show that the particle size is inversely proportional with the agitation period. The average particle size of sample S5 (141.9 nm) is approximately twice larger than that of sample S4 (61 nm). Accordingly, ultrasound application period was kept as 40 minutes.

3.2.2.2 Zeta Potential Measurements of Sample S4 and S5 at Various pH Values

The pH of the PMAA coated magnetite agglomerate solution is an important factor to provide homogeneous dispersion and to prevent agglomeration. Samples S4 and S5 were dispersed in solutions having various pH values (3.0, 6.0, 7.0, 8.0, 9.0 and 10.0) and their suspension stability in these media were followed for 14 days. For the sample S4, precipitation was not observed for 14 days. As seen in Figure 3.22 below, immediate agglomeration was observed at pH 7 for the sample $S5_{20min}$. After an observation period of 14 days, the most stable colloids were the ones dispersed at pH 3.0, 9.0 and 10.0. Therefore, it was decided that pH 3.5 was proper for dispersing the PMAA-coated magnetite nanoparticles.

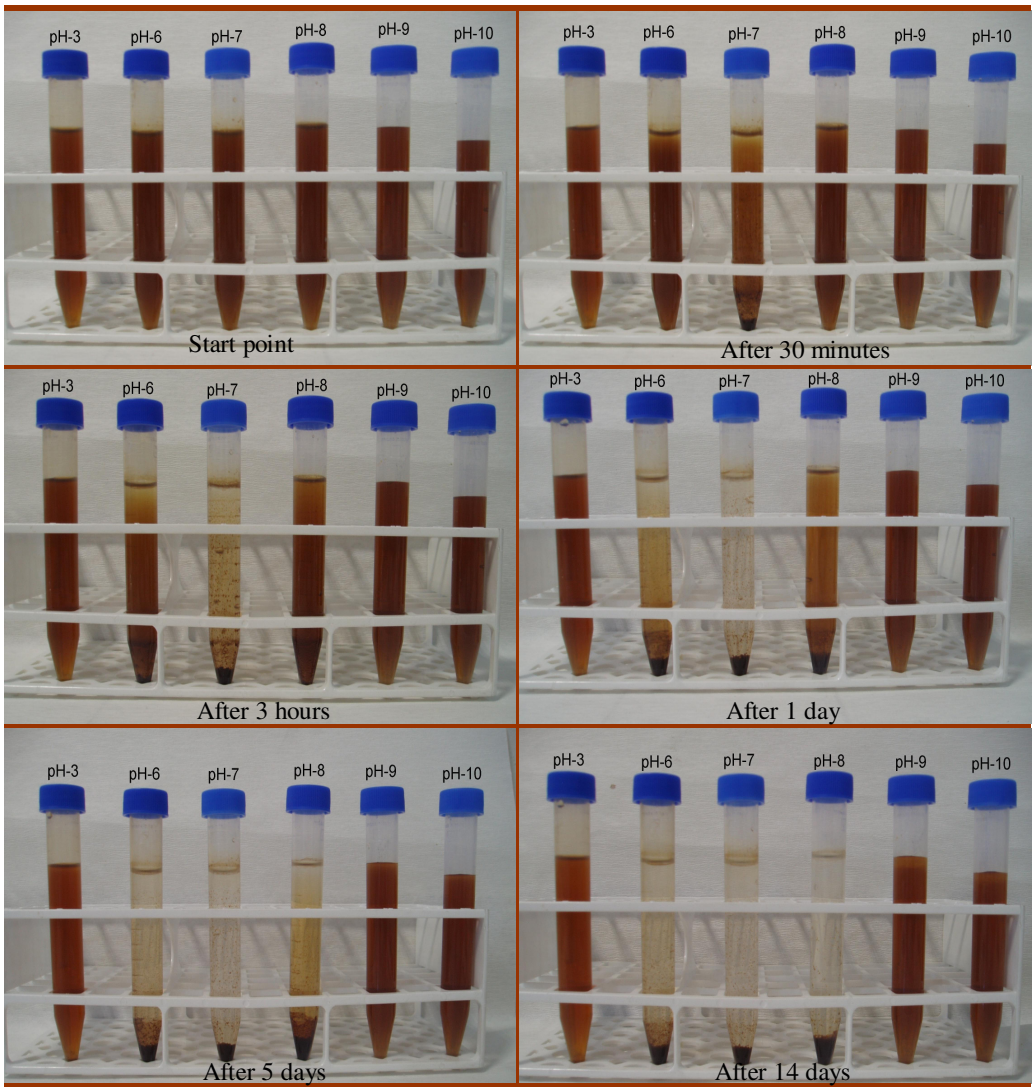

Figure 3.22 Photographs of the suspensions of S5 in solutions having various pH values after several time intervals (30 mins, 1 and 3 hours, 5 and 14 days after preparation)

The zeta potentials of S4 and S5 were measured to investigate the PMAA coating on the magnetite particles and the stability of the colloids and depicted in Figure 3.23 and Figure 3.24, respectively. The isoelectric points of S4 and S5 are pH 4.30 and pH 4.94, respectively. In literature, the isoelectric points of PMAA and magnetite was reported as approximately at pH 2.0 [102], pH 8.0 [103] respectively. The shift of the

isoelectric point from the isoelectric point of the pure magnetite, pH 8.0 to the pH 2.0 suggests that the surface of the magnetite nanoparticles was coated with PMAA efficiently.

In addition, the zeta potential of PMAA at pH 6.0 was reported as -28.0 mV [102]. As seen in the Figure 3.24 below, the zeta potential of the PMAA coated magnetite nanoparticles, S5 was found as -20 mV at pH 6. This also indicates successful PMAA coating on the surface of the magnetite nanoparticles.

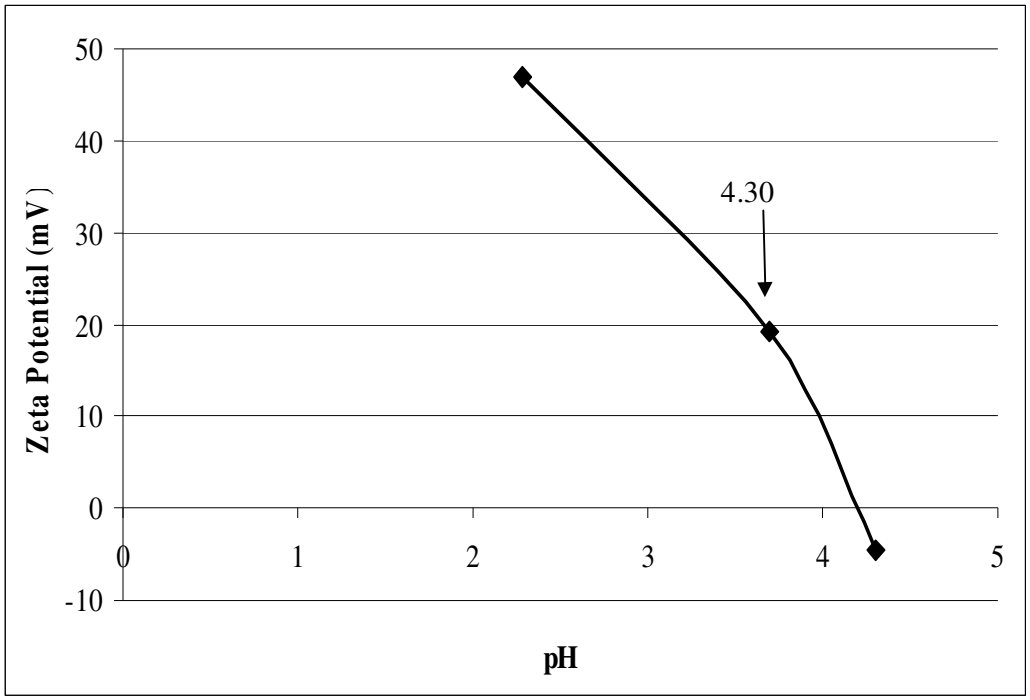

Figure 3.23 Zeta potential graph of S4, *in situ* prepared PMAA coated magnetite agglomerates under 40 minutes ultrasonic agitation.

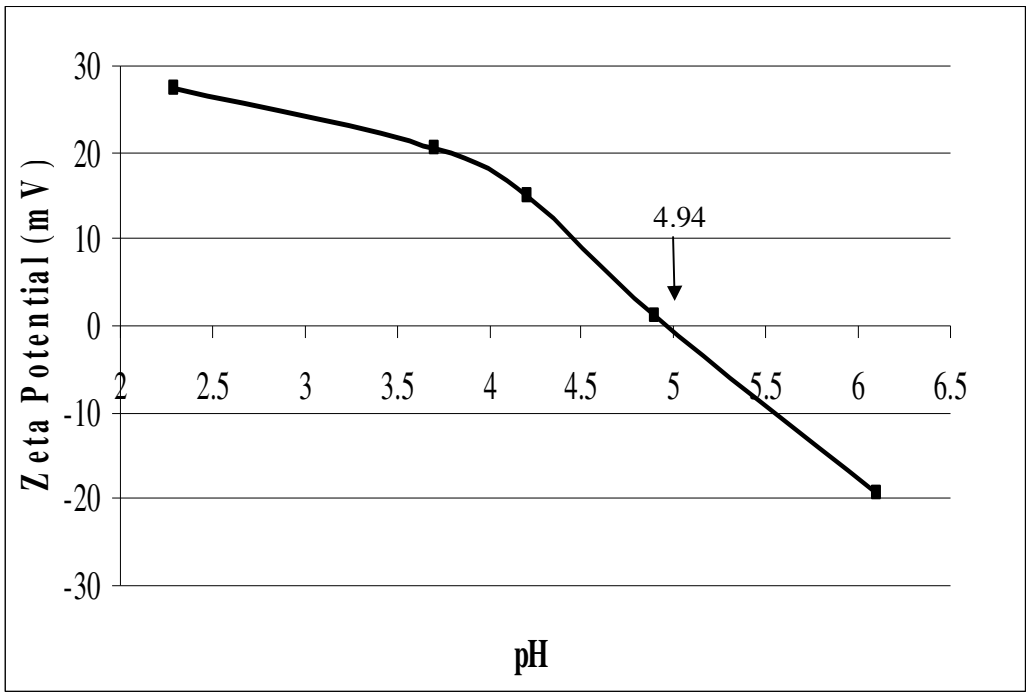

Figure 3.24 Zeta potential graph of S5, *in situ* prepared PMAA coated magnetite agglomerates under 40 minutes ultrasonic agitation

3.2.3 Magnetic Properties of Magnetite Nanoparticles and PMAA Coated Magnetite Nanoparticles

The *in situ* prepared PMAA coated magnetite agglomerates; S4 gave response to commercial magnet as clearly seen in Figure 3.25.

Figure 3.25 Magnetic property of S4, *in situ* prepared PMAA coated magnetite agglomerates under ultrasonic agitation

The magnetic properties of the magnetite nanoparticles prepared under ultrasonic agitation; S1, *in situ* prepared PMAA coated magnetite agglomerates; S4, were investigated in detail. The hysteresis loops were depicted in Figure 3.26

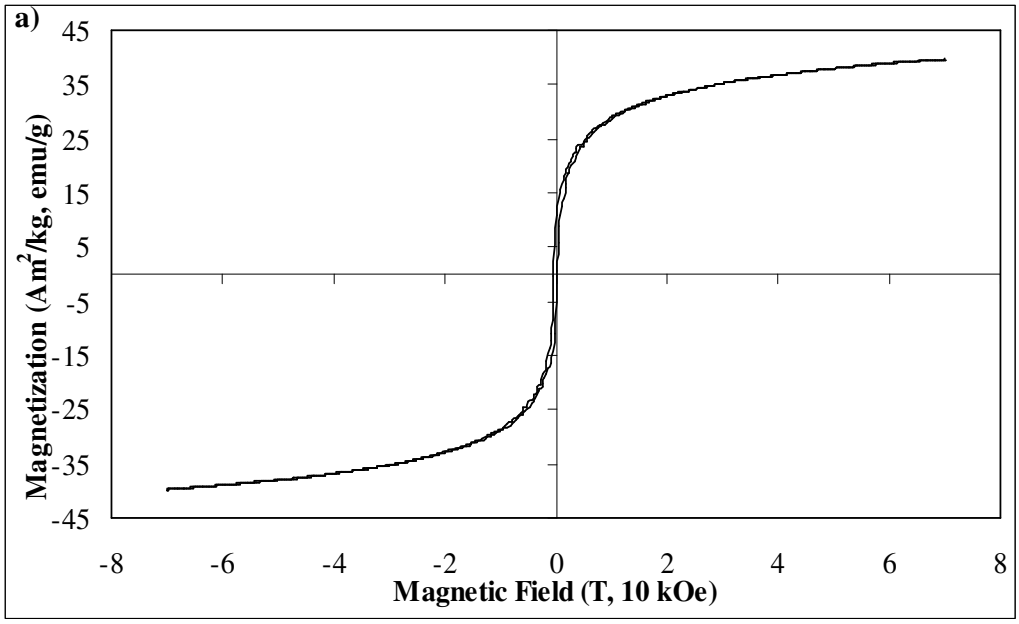

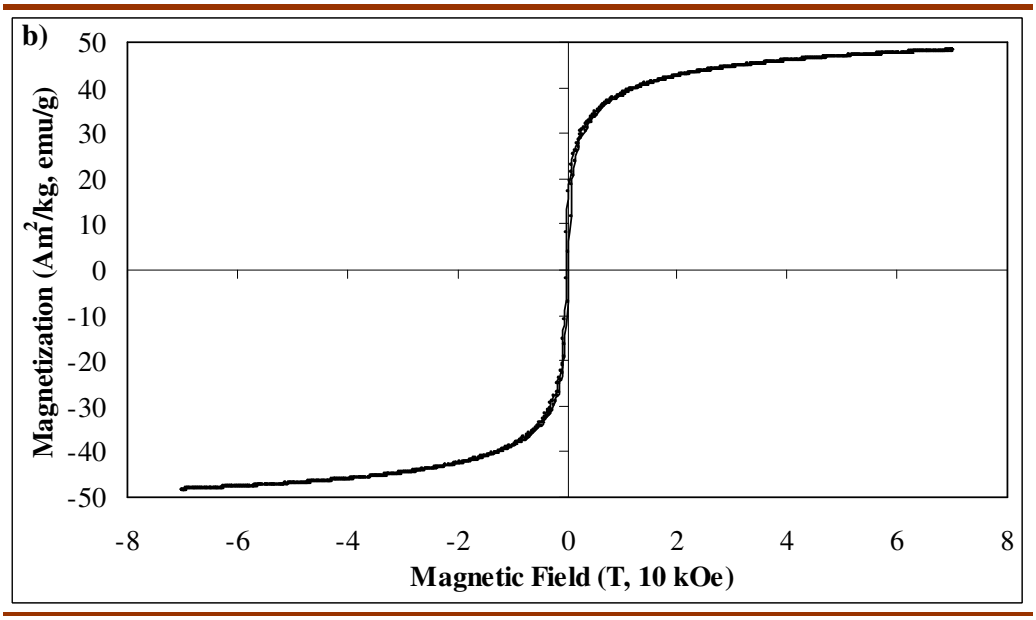

Figure 3.26 Magnetic hysteresis loops measured at 300 K of a) magnetite nanoparticles prepared under ultrasonic agitation; S1 b) *in situ* prepared PMAA coated magnetite agglomerates; S4

The magnetization curves (Figure 3.26.a and Figure 3.27.b) showed no significant hysteresis and negligible remanent magnetization and coercivity values suggesting that the magnetite nanoparticles were near superparamagnetic. The saturation magnetization values of the magnetite nanoparticles prepared under ultrasonic agitation; S1 and *in situ* prepared PMAA coated magnetite agglomerates; S4 at 300 K were determined as 39.76 emu/g and 48.29 emu/g, respectively. Even if the correction of the PMAA amount that S4 contained on the saturation magnetization value was not applied, S4 had higher saturation magnetization value. It was estimated that the reason of higher magnetization value of PMAA coated sample was that PMAA prevents magnetite nanoparticles from oxidation toward a lower saturation magnetization iron oxide phases.

The hysteresis loop of the *in situ* prepared PMAA coated magnetite agglomerates heated at 400°C was also obtained and shown in Figure 3.27 in order to investigate the effect of existence of two iron oxide phases together; magnetite and maghemite on magnetic properties.

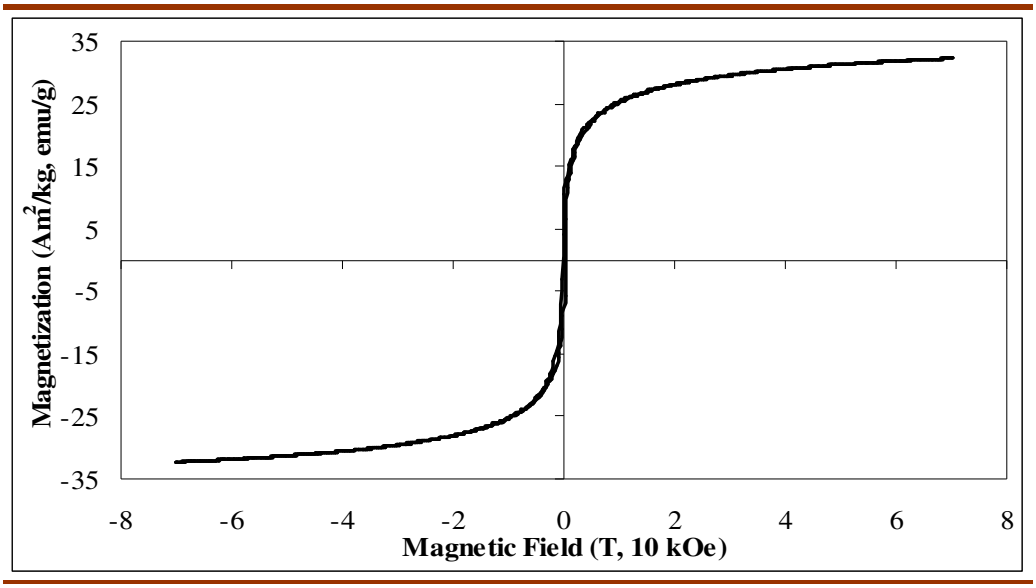

Figure 3.27 Magnetic hysteresis loop measured at 300 K of heat treated S4 at 400°C for 4 hours

The saturation magnetization values of the *in situ* prepared and heat treated at 400°C for 4 hours PMAA coated magnetite agglomerates at 300 K was determined as 32.28 emu/g. The possible reason of smaller value for saturation magnetization when compared to previous samples was the presence of two iron oxide phases; magnetite and maghemite, together which was also in good agreement with XRD spectrum of the same sample in Figure 3.15.

CHAPTER 4

CONCLUSION

In this study, two important phases of iron oxide nanoparticles were synthesized in two different respective matrices. The effects of different parameters such as precursor salts, temperature, mixing type on the particle size and the phase of iron oxide had been investigated.

Maghemite nanoparticles were synthesized in sol-gel matrix. Since nano phase of maghemite (γ-Fe_2O_3) has potential to transform different oxidation states of iron oxide, sol-gel as inert, inorganic, transparent and temperature resistant matrix was chosen to have a pure phase of maghemite with small particle size and disperse structure.

The effect of iron salt types was investigated by employing iron (III) nitrate or iron (III) chloride hexahydrate in the procedure. Between the two, using iron (III) chloride hexahydrate resulted in the hematite phase in the matrix shown by using XRD, so iron (III) nitrate nonahydrate was found to be proper for pure nano phase synthesis of maghemite in sol-gel. Later, two different calcination procedures were applied and the phases of iron oxide nanoparticles in the matrix were searched. The calcination temperature of 400 °C was found to be proper for the procedure since higher temperatures led to the hematite phase formation which was antiferromagnetic. At last, the most important factor, surface-volume ratio (S/V), which affected the final phase of iron oxide nanoparticle in the matrix, was investigated by using XRD. According to results, at high S/V, smaller particles were obtained because higher evaporation rate during the gelation had effect on the phase formation. The saturation magnetization was found to be 8 emu/g at 8 K by VSM.

Magnetite nanoparticles were coated with poly(methacrylic acid) by co-precipitation in basic solution under both magnetic stirring and ultrasonication. In order to observe the differences in agglomerate sizes and the formation of iron oxide phases, three methods were applied. Magnetite nanoparticles were synthesized with the aid of ultrasonication and characterized by XRD, SEM and zeta potential measurements. Then, PMAA-coated magnetite agglomerates with a primary particle size of approximately 9 nm were *ex situ* synthesized in two steps using both magnetic stirring and ultrasound irradiation. According to results, applying ultrasound for coating of magnetite nanoparticles with PMAA gave rise to 1000 fold decrease in agglomerate size. Finally, ultrasonication was employed for *in situ* synthesis of magnetite nanoparticles with PMAA by one-step method. The sizes of primary particle and PMAA-coated agglomerates were studied by XRD and laser particle sizer, respectively. According to the results, primary particles with 9 nm size were encapsulated in approximately 60 nm sized agglomerates. When it was compared with the reported agglomerate size values of polymer coated iron oxide nanoparticles in literature, the *in situ* synthesized PMAA coated magnetite agglomerates under ultrasonic agitation had much smaller size. Thus, the application of high intensity ultrasound during co-precipitation results in small particle size and uniform size distribution of the magnetite agglomerates in PMAA matrix. In addition, the *in situ* procedure applied at one step had advantages compared to general polymer coating methods since in these methods, the magnetic nanoparticles were synthesized separately and coated subsequently by either polymerization from monomer or chemical or physical adsorption onto the magnetic particles. The one step *in situ* procedure applied for synthesizing the iron oxide nanoparticles and coating them with PMAA at the very same time was superior to the general methods in terms of time-saving, efficiency, easeness. In addition, the uncoated and PMAA-coated magnetite nanoparticles showed near superparamagnetic magnetic properties measured by VSM. The saturation magnetization values were found to be 39.76 emu/g and 48.29 emu/g, respectively at 300 K.

REFERENCES

1 California Institute of Technology, *There's Plenty of Room at the Bottom,* http://www.its.caltech.edu/~feynman/plenty.html, last accessed on 19.06.2009.

2 Taniguchi, N. 'On the Basic Concept of 'Nano-Technology'' *Proc. Intl. Conf. Prod.* London, Part II, British Society of Precision Engineering, 1974.

3 Drexler, K. E. *Proc. Natl. Acad. Sci.* **1981**, 78, 5275.

4 Yih, T. C.; Moudgil, V. K. *Nanomedicine* **2007**, 3, 245.

5 International Risk Governance Council, *White Paper on Nanotechnology Risk Governance*, http://irgc.org/IMG/pdf/IRGC_white_paper_2_PDF_final_version-2.pdf, last accessed on 20.06.2009.

6 International Risk Governance Council, *Policy Brief on Nanotechnology Risk Governance*, http://irgc.org/IMG/pdf/PB_nanoFINAL2_2_.pdf, last accessed on 20.06.2009.

7 Center for Responsible Nanotechnology, http://www.crnano.org/, last accessed on 20.06.2009.

8 Kostoff, R. N.; Koytcheff, R. C.; Lau, C. G. Y. *J Technol Transfer* **2008**, 33, 472.

9 Sorrentino, A.; Gorrasi, G.; Vittoria, V. *Trends Food Sci. Tech.* **2007**, 18, 84

10 Yang, W.; Shen, C. Ji, Q.; An, H.; Wang, J.; Liu, Q.; Zhang, Z. *Nanotechnology* **2009**, 20, 085102.

11 Buzeaa, C.; Pacheco I. I.; Robbiec, K. *Biointerphases* **2007**, 2, MR17.

12 Burniston, N.; Bygott, C.; Stratton, J. *Surface Coat. Int. Part A* **2004**, 87, 179.

13 Ellis-Behnke, R.G.; Liang, Y.X.; You, S.W.; Tay, D.K.; Zhang, S.; So, K.F.; Schneider, G.E. *Proc Natl Acad Sci* **2006**, 103, 5054.

14 Uhrich, K.E.; Cannizzaro, S.M.; Langer, R.S.; Shakeshelf, K.M. *Chem. Rev.* **1999**, 99, 3181.

15 Harisinghani, M.G.; Barentsz, J.; Hahn, P.F.; Deserno, W.M.; Tabatabaei, S.; Hulsbergen, C.; Rosette, J.; Weissleder, R. *N. Engl. J. Medicine* **2003**, 348, 2491.

16 Palchetti, I.; Mascini, M. *Anal Bioanal Chem* **2008**, 391, 455.

17 Thompson, S.E.; Parthasarathy, S. *Mater. Today* **2006**, 9, 20.

18 Meridian Institute, *Summary of The International Workshop on Nanotechnology, Water, and Development,* http://www.merid.org/nano/waterworkshop/assets/WorkshopSummary.pdf, last accessed on 20.06.2009.

19 Shaijumon, M. M.; Reddy A. L. M.; Ramaprabhu S. *Nanosc. Res. Lett.* **2007**, 2, 75.

20 International American Society for Testing and Materials (ASTM), *Standard Terminology Relating to Nanotechnology*, http://www.astm.org/, last accessed on 20.06.2009.

21 Hosokawa, M.; Nogi, K.; Naito, M.; Yokoyama, T. *Nanoparticle Technology Handbook*, Elsevier, Amsterdam, 2007.

22 Roduner, E. *Chem. Soc. Rev.* **2006**, 35, 583.

23 Franks, A. *J. Phys. E: Sci Instrum* **1987**, 20, 1442.

24 Wu, W.; He, Q.; Jiang, C. Nanosc. Res Lett. 2008, 3, 397.

25 Parton, E.; Borghs, G.; De Palma, R. *Biomedical applications using magnetic nanoparticles*, http://www.solid-state.com/display_article/302118/5/ARTCL /none/none/Biomedical-applications-using-magnetic-nanoparticles/, last accessed on 20.06.2009.

26 Chin, A. B.; Yaacob, I. I. *J. of Mater. Process. Techn.* **2007**, 191, 235.

27 Drbohlavova, J.; Hrdy, R., Adam, V.; Kizek, R.; Schneeweiss, O.; Hubalek, J. *Sens.* **2009**, 9, 2352.

28 Laurent, S.; Forge, D.; Port, M.; Roch, A.; Robic, C.; Elst, L. V.; Muller, R. N. *Chem. Rev.* **2008**, 108, 2064.

29 Teja, A.S.; Koh, P. Y. *Prog. Crys. Growth Charac. of Mater.*. **2009**, 55, 22.

30 Cornell, R. M.; Schwertmann, U. 'The Iron Oxides: Structure, Properties, Reactions, Occurrences and Uses'; Second Edition, Wiley-VCH, Weinheim, 2003.

31 Georgia State University, http://hyperphysics.phy-astr.gsu.edu/Hbase/solids/hyst.html#c1, last accessed on 21.06.2009.

32 The NTD Resource Center, http://www.ndt-ed.org/EducationResources/CommunityCollege/MagParticle/Physics/HysteresisLoop.htm, last accessed on 21.06.2009.

33 Mineralogy Database, http://www.webmineral.com/, last accessed on 20.06.2009.

34 Cabrera, L.; Gutierrez, S.; Menendez, N.; Morales, P. M.; Herrasti, P. *Electrochim. Acta* **2008**, 53, 3436.

35 Wu, J.; Ko, P. S.; Liu, H.; Kim, S.; Ju, J.; Kim, K. Y. *Mater. Lett.* **2007**, 61, 3124.

36 Xu, J.; Yang, H.; Fu, W.; Du, K.; Sui Y.; Chen, J.; Zeng, Y.; Li M.; Zou, G. *J Magn. Magn. Mater.* **2007**, 309, 307.

37 Mi, W. B.; Shen J. J.; Jiang E. Y. *Bio Acta Mater.* **2007**, 55, 1919.

38 Alvarez, M.; Rueda, E. H.; Sileo, E. E. *Chem. Geol.* **2006,** 231, 288.

39 Kluchova, K.; Zboril, R.; Tucek, J.; Pecova, M.; Zajoncova, L.; Safarik, I.; Mashlan, M.; Markova, I.; Jancik, D.; Sebela, M.; Bartonkova, H.; Bellesi, V.; Novak, P.; Petridis, D. *Biomaterials* **2009**, 30, 2855.

40 Sun, Y.; Ma, M.; Zhang, Y.; Gu, N. *Colloid and Surface A* **2004***,* 245, 15.

41 Lyklema, J. 'Fundamentals of Interface and Colloid Science', Vol. 2, Academic Press, London/San Diego/New York, 1995.

42 Lattuada, M.;Hatton, A.T. *Langmuir* **2007**, 23, 2158.

43 Hong, J.; Xu, D.; Yu,J.; Gong, P.; Ma, H.; Yao, S. *Nanotechnology* **2007**, 18, 135608.

44 Suslick, K. S.; Flannigan, D. J. *Annu. Rev. Phys. Chem.* **2008**, 59, 659.

45 Suslick, K. S.; Price, J. P. *Annu. Rev. Mater. Sci.* **1999**, 29, 295.

46 Vidal-Vidal J.; Rivas, J.; L´opez-Quintela, A M. *Colloid and Surface A* **2006**, 288, 44.

47 You , X. C.; Zhang C. J.; Shen, Y.; Song, W. Z. *Acta Metall. Sin.* **2007**, 20, 434.

48 Sun, S.; Zeng, H. *J. Am Chem Soc.* **2002**, 124, 8204.

49 Choi, C. J.; Dong, X. L.; Kim, B. K. *Mater Trans.* **2001**, 42, 2046.

50 Zhang, G.; Shen, K.; Zhao, D.; Yuan, Y.; Wang, G. *Mater. Lett.* **2008**, 62, 219.

51 Kim, H. Ki.; Kim M.; Choa, Y.; Kim, H D.; Yu, J. *IEEE Trans. Magn.* **2008**, 44, 2940.

52 Sun, Y.; Duan, L.; Guo, Z.; DuanMu, Y.; Ma M.; Xu, Li.; Zhang, Y.; Gu, N. *J. Magn. Magn. Mater.* **2005**, 285, 65.

53 Sakka, S. 'Handbook of Sol-gel Science And Technology: Processing, Characterization, and Applications', Kluwer Academic Publishers, Boston, 2004.

54 Bréchignac, C.; Houdy, P.; Lahmani, M. 'Nanomaterials and Nanochemistry' Springer, New York, 2008.

55 Camponeschi, E.; Walker, J.; Garmestani, H.; Tannenbaum, R. *J. Non-Cryst. Solids* **2008**, 354, 4063.

56 Yang, D.; Hu, J.; Fu, S. *J. Phys. Chem. C* **2009,** *113,* 7646.

57 Xu , X.; Wang, J.; Yang, C.; Wu, H.; Yang, F. *J. of Alloy Compd.* **2009**, 468, 414.

58 Solinas, S.; Piccaluga, G.; Morales, M. P.; Serna, C. J. *Acta mater.* **2001**, 49, 2805.

59 Savii, C.; Popovici, M.; Enache, C.; Subrt, J. *Solid State Ion.* **2002**, 151, 219.

60 Tao; S.; Liu, X.; Chu, X.; Shen, Y. *Sens. and Actuator. B* **1999**,61, 33.

61 Caizer, C.; Savii, C.; Popovici, M. *Mater. Sci. Eng. B* **2003**, 97, 129.

62 Mukadam, M. D.; Yusuf, S. M.; Sharma, P.;Kulshreshtha, S. K. *J. Magn.Magn. Mater.* **2004**, 272, 1401.

63 Hseih, C. T.; Huang, W. L.; Lue, J. T. *J. Phys. Chem. Solids* **2002**, 63, 733.

64 Iwasaki, T.; Kosaka, K.; Mizutania, N.; Watano, S.; Yanagida, T.; Tanaka, H.; Kawai, T. *Mater. Lett.* **2008**, 62, 4155.

65 Jeong, J.; Shin, S.; Lee, S.; Kim, K. *J. Magn.Magn. Mater.* **2005**, 286, 5.

66 Majewski, P.; Thierry, B. *Crit. Rev. Solid State* **2007**, 32, 203.

67 Khaleel, A. A. *Chem. A Eur. J.* **2004**, 10, 925.

68 Chastellain, A.; Petri , A.; Hofmann, H. *J. Colloid Interf. Sci* **2004,** 278, 353.

69 Tamaura, Y.; Ito, K.; Katsura, T. *J. Chem. Soc. Dalton Trans.* **1983**, 2, 189.

70 Tronc, E.; Belleville, P.; Jolivet, J. P.; Livage, J. *Langmuir* **1992**, 8, 313.

71 Jolivet, J. P.; Tronc, E. *J. Colloid Interf. Sci.* **1988**, 28, 688.

72 Sugimoto, T.; Matijevic, E. *J. Colloid Interf. Sci.* **1980**, 74, 227.

73 Tartaj, P.; Gonzalez-Carreno, T.; Bomatı-Miguel, O.; Serna, J. C. *Phys. Rev. B* **2004**, 69, 094401.

74 Burke, D. A. N.;. Stöver, H. D. H.; Dawson P. F. *Chem. Mater.* **2002**, 14, 4752.

75 Reddya, R. K.; Parka, W.; Sina, C. B.; Nohb, J.; Lee, Y. *J. Colloid Interf. Sci*. **2009***,* 335, 34.

76 Gyergyek, S.; Huskić, M.; Makovec, D.; Drofenik, M. *Colloid Surfaces A* **2008**, 317, 49.

77 Nitin, N.; LaConte, W. E. L.; Zurkiya, O.; Hu, X.; Bao, G. *J Biol Inorg Chem.* **2004**, 9, 706.

78 Zaitsev, S. V.; Filimonov, S. D.; Presnyakov, A. I.; Gambino, J. R.; Chu, B. *J. Colloid Interf. Sci.* **1999**, 212, 49.

79 Wan, M.; Li, J. *J. Polymer. Sci*. **1998**, 36, 2799.

80 Butterworth, M. D.; Bell, S. A.; Armes, S. P.; Simpson, A.W. *J. Colloid Interf. Sci*. **1996**, 183, 91.

81 Tartaj, P.; Morales, M. P.; Gonzalez-Carreno, T.; Veintemillas- Verdaguer, S.; Serna, C. J. *J. Magn. Magn. Mater.* **2005**, 28, 290.

82 Barratt, G. *Cell. Mol. Life Sci*. **2003**, 60, 21.

83 Landfester, K.; Ramirez, L. P. *J. Phys.: Condens. Matter* **2003**, 15, S1345.

84 Liu, L. Z.; Ding, H. Z.; Yao, L. K.; Tao, J.; Du, H. G.; Lu, H. Q.; Wang, X.; Gong, L. F.; Chen X.; *J. Magn. Mag. Mater.* **2003**, 265, 98.

85 Huang, J.; Wan, S.; Guo, M.; Yan, H. *J. Mater. Chem*. **2006**, 16, 4535.

86 Gass, J.; Poddar, P.; Almand, J.; Srinath, S.; Srikanth, H. *Adv. Funct. Mater.* **2006**, 16, 71.

87 Tural, B.; Özkan, N.; Volkan, M. *J. Phys. Chem. Solids* **2009**, 70, 860.

88 Zhang, Q. G.; Wu, P. H.; Ge, Y. M.; Jiang, K. Q.; Chen, Y. L.; Yao M. J. *Mater. Lett.* **2007**, 61, 2204.

89 Mizukoshi Y.; Shuto T.; Masahashi N.; Tanabe S. *Ultrason. Sonochem.* **2009**, 16, 525

90 Gedanken, A. *Ultrason. Sonochem.* **2007**, 14, 418.

91 Cheetham, A. K.; Day, P. 'Solid State Chemistry Techniques', Clarendon Press, Oxford, 1987.

92 Flynn, C. M. *Chem. Rev.* **1984**, 84, 31.

93 Music, S.; Vertes, A.; Simmons, G. W.; Czako-Nagy I.; Leidheiser, H. *J. Colloid Interf. Sci.* **1982**, 85, 256.

94 Morales, M. P.; Gonzalez-Carreno T.; Serna, C. J. *J. Mater. Res*. **1992,** 7, 2538.

95 Murphy, P. J.;. Posner A. M; Quirk, J. P. *J. Colloid Interf. Sci.* **1976,** 56, 312.

96 Solinas, S.; Piccaluga, G.; Morales, M. P.; Serna, C. J. *Acta Mater.* **2001**, 49, 2805

97 Berkowitz, A. E.; Schuele, W. J.; Flanders, P. J. *J. Appl. Phys.* **1968**, 39, 1261.

98 Martinez, B.; Roig, A.; Obradors, X.; Mollins, E.; Rouanet, A.; Monty, C. *J. Appl. Phys*, **1996,** 79, 2580.

99 Tural, B.; Kaya, M.; Özkan, N.; Volkan, M. *J. Nanosci. Nanotech.* **2008**, 8, 695.

100 Alibeigi, S.; Vaezi, R. M.; *Chem. Eng. Technol.* **2008**, 31, 11, 1591.

101 Suryanarayana, C. 'Mechanical. Alloying and. Milling', Marcel Dekker, New York, 2004.

102 Yu, S.; Chow, M. G. *J. Mater. Chem.* **2004**, 14, 2781.

103 Illés, E.; Tombácz, E. *J. Colloid Interf. Sci.* **2006**, 295, 115.